Study of the process $e^+e^-\to\pi^+\pi^-\pi^0$ in the energy region $\sqrt{s}$ below 0.98 GeV

M. N. Achasov,* K. I. Beloborodov, A. V. Berdyugin, A. G. Bogdanchikov, A. V. Bozhenok, A. D. Bukin, D. A. Bukin, T. V. Dimova, V. P. Druzhinin, V. B. Golubev, I. A. Koop, A. A. Korol, S. V. Koshuba, A. P. Lysenko, E. V. Pakhtusova, S. I. Serednyakov, V. V. Shary, Yu. M. Shatunov, Z. K. Silagadze, A. N. Skrinsky, A. A. Valishev, and A. V. Vasiljev

Budker Institute of Nuclear Physics, Siberian Branch of the Russian Academy of Sciences and Novosibirsk State University, 11 Lavrentyev, Novosibirsk, 630090, Russia

(Received 20 May 2003; published 30 September 2003)

The cross section of the process $e^+e^-\to\pi^+\pi^-\pi^0$ was measured in the Spherical Neutral Detector (SND) experiment at the VEPP-2M collider in the energy region $\sqrt{s}$ below 980 MeV. This measurement was based on about 1.2×10^6 selected events. The obtained cross section was analyzed together with the SND and DM2 data in the energy region $\sqrt{s}$ up to 2 GeV. The ω-meson parameters $m_\omega=782.79\pm0.08\pm0.09$ MeV, $\Gamma_\omega=8.68\pm0.04\pm0.15$ MeV, and $\sigma(\omega\to3\pi)=1615\pm9\pm57$ nb were obtained. It was found that the experimental data cannot be described by a sum of only ω, ϕ, ω', and ω'' resonance contributions. This can be interpreted as a manifestation of $\rho\to3\pi$ decay, suppressed by G parity, with a relative probability $B(\rho\to3\pi)=(1.01^{+0.54}_{-0.36}\pm0.034)\times10^{-4}$.

DOI: 10.1103/PhysRevD.68.052006 PACS number(s): 13.66.Bc, 12.40.Vv, 13.25.Jx, 14.40.Cs

I. INTRODUCTION

The cross section of the $e^+e^-\to\pi^+\pi^-\pi^0$ process in the energy region $\sqrt{s}<2$ GeV is determined by the transitions of light vector mesons $V(V=\omega,\phi,\omega',\omega'')$ into the final state: $V\to\pi^+\pi^-\pi^0$. The $V\to\pi^+\pi^-\pi^0$ branching ratios for vector mesons with isospin $I=0$ are large, $B(\omega\to3\pi)\simeq0.9$, $B(\phi\to3\pi)\simeq0.15$ [1], $B(\omega'\to3\pi)\sim1$, $B(\omega''\to3\pi)\sim0.5$ [2], and thus the $e^+e^-\to\pi^+\pi^-\pi^0$ cross section measurements are important for the study of these resonances. The $\rho\pi$ intermediate state dominates in these transitions. The $V\to\pi^+\pi^-\pi^0$ transition can also proceed via mechanisms suppressed by the G parity: $V\to\omega\pi^0\to\pi^+\pi^-\pi^0$ [2,3] or $V\to\rho\pi\to\pi^+\pi^-\pi^0$ $(V=\rho,\rho',\rho'')$. Studies of the $e^+e^-\to\pi^+\pi^-\pi^0$ reaction allow us to determine the vector meson parameters and provide information on the Okubo-Zweig-Iizuka (OZI) rule violation in $\phi\to3\pi$ decay and on the G-parity violation in the processes $\rho,\rho'^{(\prime\prime)}\to3\pi$.

The process $e^+e^-\to\pi^+\pi^-\pi^0$ in the energy region $\sqrt{s}$ below 2200 MeV was studied in several experiments during the last 30 years. The ω meson production region was studied in Refs. [4–10] and studies of the ϕ meson energy domain were reported in Refs. [8,11–16]. In Refs. [8,17–19] the $e^+e^-\to\pi^+\pi^-\pi^0$ cross section was studied in the wide energy region $\sqrt{s}$ from 660 up to 1100 MeV and in Ref. [20] an upper limit was imposed on the G-parity suppressed decay $\rho\to3\pi$. $e^+e^-\to\pi^+\pi^-\pi^0$ cross section measurements in the ω' and ω'' resonance energy region ($\sqrt{s}=1100$–2200 MeV) were reported in Refs. [8,19,21–25].

Recently, the process $e^+e^-\to\pi^+\pi^-\pi^0$ was also studied with the Spherical Neutral Detector (SND) [2,26–28], the process dynamics was analyzed, and the cross section was measured in the energy region $\sqrt{s}$ from 980 to 1380 MeV. Here we present the $e^+e^-\to\pi^+\pi^-\pi^0$ cross section measurement in the energy region $\sqrt{s}$ below 980 MeV. The cross section obtained was analyzed together with the SND [2,27] and DM2 [25] data in the energy region up to 2000 MeV.

II. EXPERIMENT

The SND detector [29] operated from 1995 to 2000 at the VEPP-2M [30] collider in the energy range $\sqrt{s}$ from 360 to 1400 MeV. The detector contains several subsystems. The tracking system includes two cylindrical drift chambers. The three-layer spherical electromagnetic calorimeter is based on NaI(Tl) crystals. The muon/veto system consists of plastic scintillation counters and two layers of streamer tubes. The calorimeter energy and angular resolutions depend on the photon energy as $\sigma_E/E(\%)=4.2\%/\sqrt[4]{[4E(\mathrm{GeV})}$ and $\sigma_{\phi,\theta}=0.82°/\sqrt{E(\mathrm{GeV})}\oplus0.63°$. The tracking system angular resolution is about 0.5° and 2° for azimuthal and polar angles, respectively.

In 1998–2000 the SND detector collected data in the energy region $\sqrt{s}<980$ MeV with integrated luminosity about 10.0 pb^{-1}. For the luminosity measurements, the processes $e^+e^-\to e^+e^-$ and $e^+e^-\to\gamma\gamma$ were used. In this work the luminosity measured by using $e^+e^-\to\gamma\gamma$ was used for normalization, because in the ρ meson energy region the contribution of the $e^+e^-\to\pi^+\pi^-$ background to the $e^+e^-\to e^+e^-$ process is rather large. The systematic error of the integrated luminosity determination is estimated to be 2%. Since luminosity measurements by $e^+e^-\to e^+e^-$ and $e^+e^-\to\gamma\gamma$ reveal a systematic spread of about 1%, this was added to the statistical error of the luminosity determination at each energy point. The statistical accuracy was better than 1%.

The beam energy was calculated from the magnetic field value in the bending magnets and the revolution frequency of the collider. The relative accuracy of the energy setting for each energy point is about 0.1 MeV, while the common shift of the energy scale for all points within the scan can amount

*Email address: achasov@inp.nsk.su

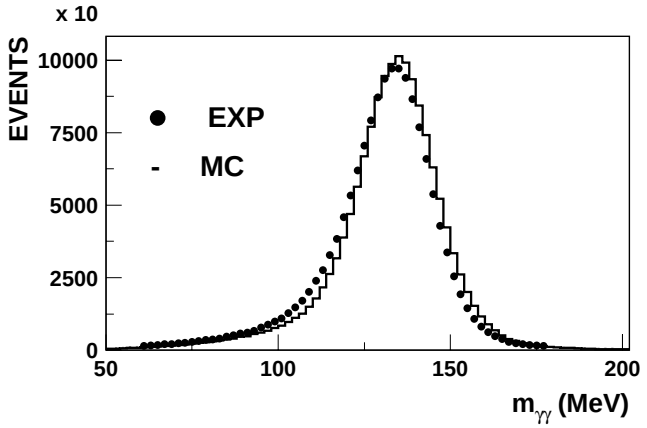

FIG. 1. Two-photon invariant mass distribution in the $e^+e^- \to \pi^+\pi^-\pi^0$ events.

to 0.5 MeV. At the three energy points in the vicinity of the ω resonance peak the beam energy was calibrated using the resonant depolarization method [31]. The accuracy of the center of mass energy calibration is 0.04 MeV. In order to correct the calculated beam energy, the common shifts of the energy scale in the experimental scans were the free parameters in the analysis and varied relative to the calibrated energy points. The beam energy spread varies in the range from 0.08 MeV at $\sqrt{s}=440$ MeV to 0.35 MeV at $\sqrt{s}=970$ MeV.

III. DATA ANALYSIS

A. Selection of $e^+e^- \to \pi^+\pi^-\pi^0$ events

The data analysis and selection criteria used in this work are similar to those described in Refs. [2,27,28]. During the experimental runs, the first-level trigger [29] selects events with energy deposition in the calorimeter greater than 180 MeV and with two or greater charged particles. During processing of the experimental data the event reconstruction is performed [27,29]. For further analysis, events containing two or more photons and two charged particles with $|z|<10$ cm and $r<1$ cm were selected. Here z is the coordinate of the charged particle production point along the beam axis (the longitudinal size of the interaction region depends on beam energy and varies from 2 to 2.5 cm); r is the distance between the charged particle track and the beam axis in the r-ϕ plane. Extra photons in $e^+e^- \to \pi^+\pi^-\pi^0$ events can appear because of the overlap with the beam background or nuclear interactions of the charged pions in the calorimeter. Under these selection conditions, the background sources are the $e^+e^- \to \omega\pi^0 \to \pi^+\pi^-\pi^0\pi^0$, $e^+e^- \to e^+e^-\gamma$, $e^+e^- \to \gamma\gamma$, $\pi^+\pi^-(\gamma)$, $\mu^+\mu^-(\gamma)$ processes, and cosmic and beam backgrounds.

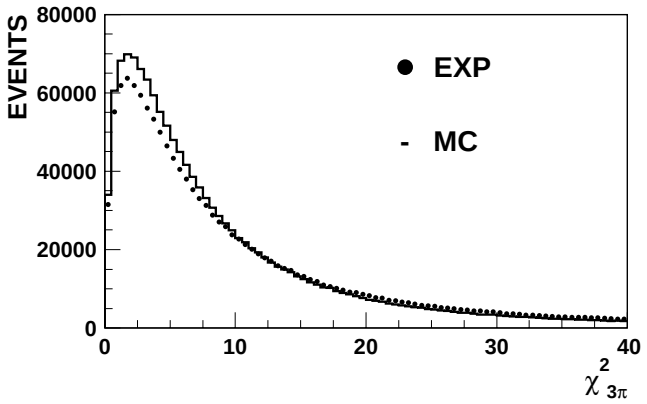

FIG. 2. The $\chi^2_{3\pi}$ distribution in the $e^+e^- \to \pi^+\pi^-\pi^0$ events.

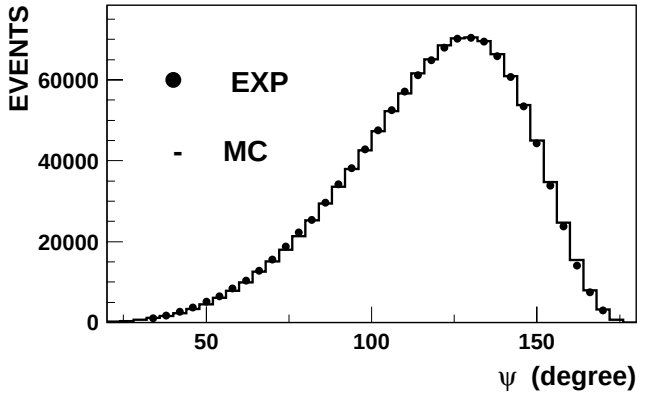

FIG. 3. Angle ψ between the charged pions in the $e^+e^- \to \pi^+\pi^-\pi^0$ events.

The polar angles of the charged particles were bounded by the criterion $15° < \theta < 165°$. To suppress the cosmic and beam backgrounds, the following cuts were applied: $E_{neu} > 100$ MeV, $2 \leqslant N_\gamma \leqslant 3$, $|\Delta z| < 3$ cm, and $\psi > 20°$. Here E_{neu} is the energy deposition of the neutral particles, N_γ is the number of detected photons, $\Delta z = z_1 - z_2, z_1, z_2$ are the z coordinates of the charged particle tracks, and ψ is the angle between two charged particle tracks.

To suppress the $e^+e^- \to e^+e^-\gamma\gamma$ events, the energy deposition of the charged particles in the calorimeter, E_{cha}, was required to be small: $E_{cha} < 0.5 \cdot \sqrt{s}$.

To reject the background from $e^+e^- \to \pi^+\pi^-(\gamma)$, $\mu^+\mu^-(\gamma)$, and $e^+e^-\gamma$, the following cut was imposed: $|\Delta\phi| > 5°$. Here $\Delta\phi$ is the acollinearity angle of the charged particles in the azimuthal plane.

When these cuts were imposed, the number of background events decreased by a factor of about 10, while the

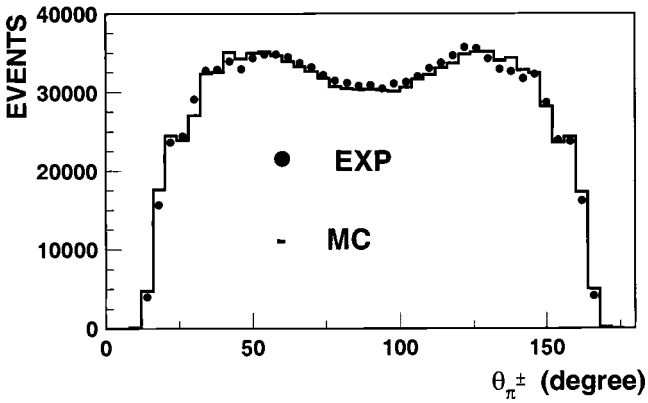

FIG. 4. The θ distribution of charged pions from the reaction $e^+e^- \to \pi^+\pi^-\pi^0$.

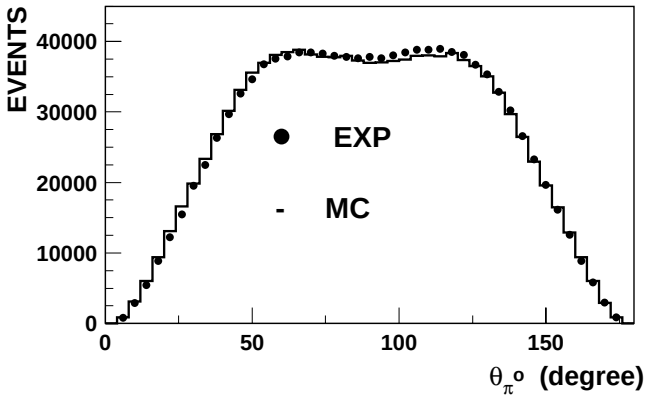

FIG. 5. The θ distribution of neutral pions from the reaction $e^+e^-\to\pi^+\pi^-\pi^0$.

number of $e^+e^-\to\pi^+\pi^-\pi^0$ reaction events decreased by only about 10%.

For the events left after these cuts, a kinematic fit was performed under the following constraints: the charged particles are assumed to be pions, the system has zero total momentum, the total energy is $\sqrt{s}$, and the photons originate from the $\pi^0\to\gamma\gamma$ decays (Fig. 1). The value of the likelihood function $\chi^2_{3\pi}$ (Fig. 2) is calculated during the fit. In events with more than two photons, extra photons are considered as spurious ones and rejected. To do this, all possible subsets of two photons were inspected and the one corresponding to the maximum likelihood was selected. The kinematic fits were also performed under the assumptions that the $e^+e^-\to\pi^+\pi^-\gamma$, $e^+e^-\to\mu^+\mu^-\gamma$, or $e^+e^-\to e^+e^-\gamma$ events with extra photons were detected and the values of the corresponding likelihood functions $\chi^2_{2\pi\gamma}$, $\chi^2_{2\mu\gamma}$, and $\chi^2_{2e\gamma}$ were calculated. After the kinematic fits, the following cuts were applied: $\chi^2_{3\pi}<20$, $\chi^2_{2\pi\gamma}>20$, $\chi^2_{2\mu\gamma}>20$, and $\chi^2_{2e\gamma}>20$, the polar angle θ_γ of at least one of the photons, selected by the reconstruction program as originating from the π^0 decay, should satisfy the following criterion: $36°<\theta_\gamma<144°$. In the energy region $\sqrt{s}<730$ MeV, for additional suppression of the background, the cut $p/E>0.5$–0.3 (at $\sqrt{s}=720$–440 MeV) was applied. Here p and E are the

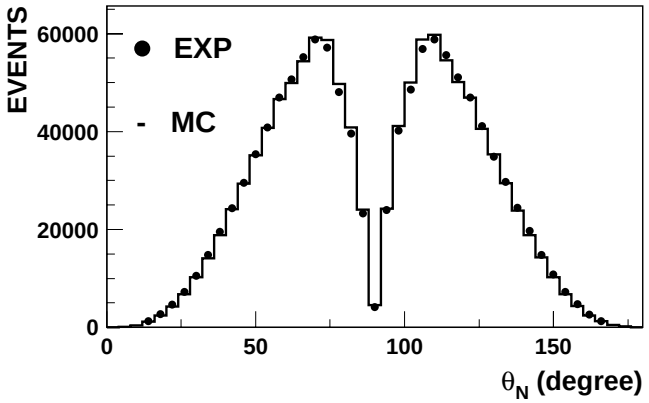

FIG. 6. The angle between the normal to the production plane and the e^+e^- beam direction for the $e^+e^-\to\pi^+\pi^-\pi^0$ events.

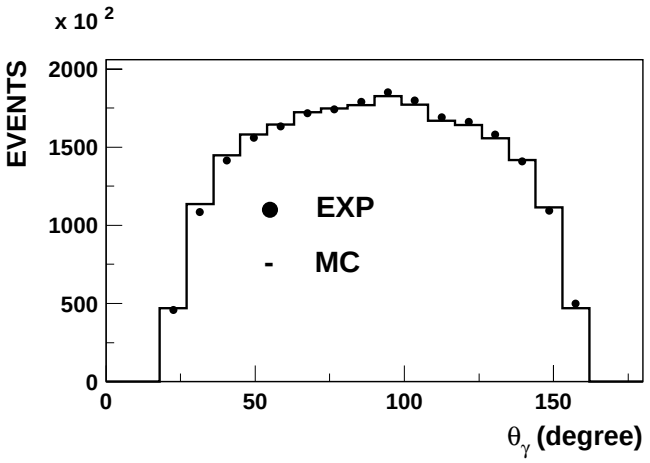

FIG. 7. The angular distribution of photons.

charged pion momentum and energy calculated after the kinematic reconstruction. For additional suppression of the $e^+e^-\to\omega\pi^0\to\pi^+\pi^-\pi^0\pi^0$ background, the criterion $N_\gamma=2$ was applied for energies $\sqrt{s}>900$ MeV. As a result of the applied cuts the background was suppressed by about 1000 times.

The angular distributions of particles for the selected events are shown in Figs. 3–7, while Figs. 8–11 demonstrate the photon and pion energy distributions for the same events. The experimental and simulated distributions are in agreement.

B. Background subtraction

The number of background events was estimated from the following formula:

$$N_{bkg}(s)=\sum_i \sigma_{Ri}(s)\epsilon_i(s)\mathcal{L}(s), \tag{1}$$

where i is the process number, $\sigma_{Ri}(s)$ is the cross section of the background process taking into account the radiative corrections, $\mathcal{L}(s)$ is the integrated luminosity, and $\epsilon_i(s)$ is the detection probability for the background process obtained from a simulation under the selection criteria described

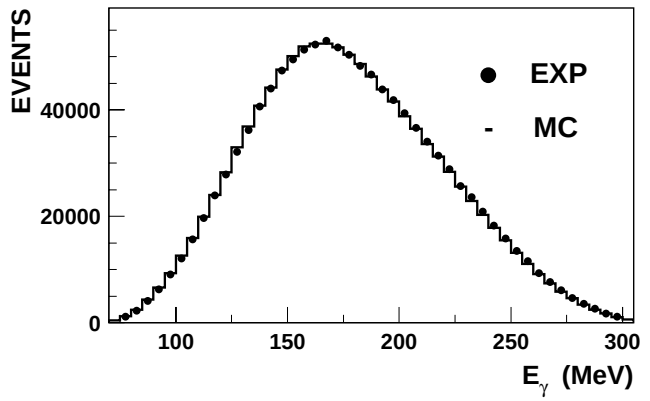

FIG. 8. The energy distribution for the most energetic photon.

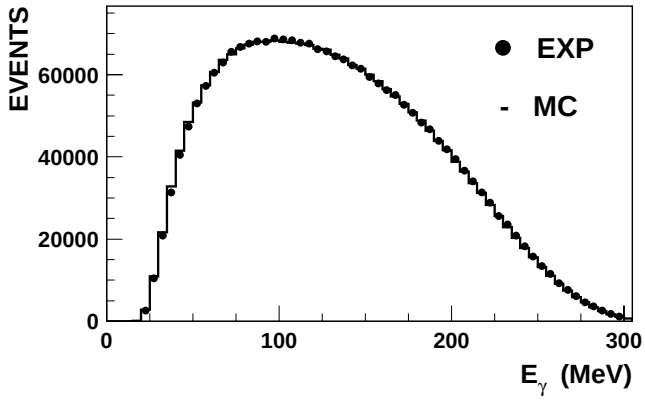

FIG. 9. The photon energy distribution.

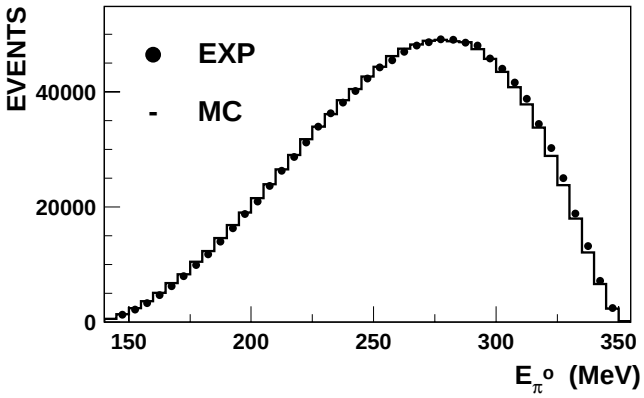

FIG. 11. The neutral pion energy distribution.

above. For the $e^+e^-\to\omega\pi$ background estimation, the cross section obtained in SND experiments [32] was used.

To estimate the accuracy of the background event number determination, the $\chi^2_{3\pi}$ distribution in the energy region $\sqrt{s}>870$ MeV was studied (Fig. 12). The experimental $\chi^2_{3\pi}$ distribution in the range $0<\chi^2_{3\pi}<40$ was fitted by a sum of background and signal. The distribution for background events was taken from the simulation, and for the signal $e^+e^-\to\pi^+\pi^-\pi^0$ events by using experimental data collected in the vicinity of the ω meson peak. As a result, the ratio between the number of background events obtained from the fit and the number calculated according to Eq. (1) was found to be 2.0 ± 1.2. The error was estimated by varying the selection criteria. Taking this ratio into account, the number of background events obtained from Eq. (1) was multiplied by a factor of 2 at all energy points and the accuracy of the determination of the number of background events was estimated to be about 60%.

The numbers of $e^+e^-\to\pi^+\pi^-\pi^0$ events (after the background subtraction) and background event numbers are shown in Table I.

To check the accuracy of background subtraction in the energy region $\sqrt{s}<730$ MeV, the data were analyzed in a different way. The kinematic reconstruction was performed under the following constraints: the charged particles are pions, the system has zero total momentum, and the total energy is $\sqrt{s}$. The constraint that the photon originated from the $\pi^0\to\gamma\gamma$ decay was not used. In events with more than two photons, extra photons are considered as spurious ones and rejected. The value of the likelihood function $\chi^2_{2\pi2\gamma}$ is calculated during the fit. After the fit, the following cut was applied: $\chi^2_{2\pi2\gamma}<20$. For selected events the two-photon $m_{\gamma\gamma}$ invariant mass spectra (Fig. 13) were fitted by a sum of background and signal ($m_{\gamma\gamma}$ is calculated after the kinematic fit). The shape of the distribution for $e^+e^-\to\pi^+\pi^-\pi^0$ events was obtained by using experimental data collected in the vicinity of the ω resonance. For the background a uniform distribution was used (other assumptions about the shape of the background spectrum do not change the fit results). The cross sections obtained by using two different methods of background subtraction are in agreement (Table II). An analogous check was performed for the energy region $\sqrt{s}>900$ MeV. The results of the different approaches are again in agreement.

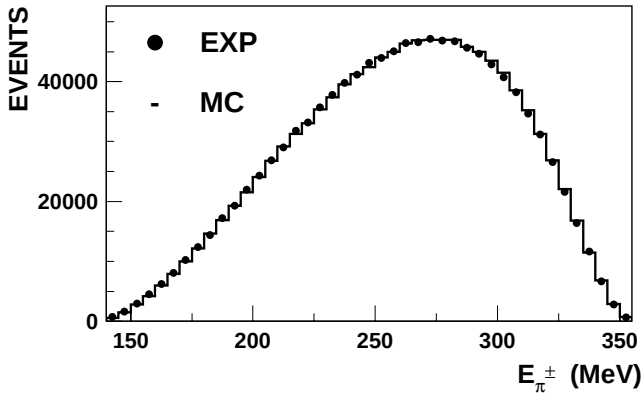

FIG. 10. The charged pion energy distribution.

C. Detection efficiency

The detection efficiency of the $e^+e^-\to\pi^+\pi^-\pi^0(\gamma)$ process was obtained from simulation. To take into account the overlap of the beam background with the signal events, background events (experimental events collected when the

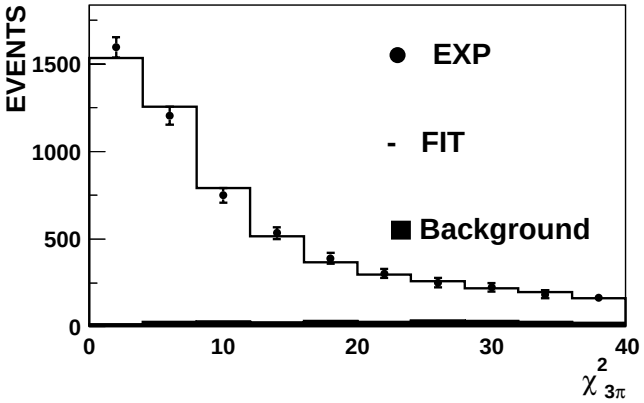

FIG. 12. The experimental $\chi^2_{3\pi}$ distribution in the energy region $\sqrt{s}>870$ MeV, fitted by the sum of distributions for the signal and background. The background contribution is shown by the filled histogram.

TABLE I. Event numbers $N_{3\pi}$ of the $e^+e^- \to \pi^+\pi^-\pi^0(\gamma)$ process (after background subtraction) and N_{bkg} of background processes, integrated luminosity $\mathcal{L}$, and detection efficiency $\epsilon(s,E_\gamma=0)$ (without γ quantum radiation). δ_{rad} is the radiative correction [$\delta_{rad}=\xi(s)/\epsilon(s,E_\gamma=0)$, $\xi(s)$ is defined via expression (19)].

$\sqrt{s}$ (MeV)	$\mathcal{L}$ (nb^{-1})	$\epsilon(s,E_\gamma=0)$	$N_{3\pi}$	N_{bkg}	δ_{rad}
970	271.4±2.7	0.2544±0.0082	800±34	33±7	0.905
958	249.0±2.5	0.2544±0.0082	658±29	27±5	0.918
950	276.8±2.7	0.2540±0.0086	727±32	32±6	0.927
940	505.2±4.5	0.2585±0.0075	1203±41	53±10	0.937
920	510.1±4.1	0.2699±0.0075	1292±42	52±8	0.96
880	397.6±3.6	0.3268±0.0032	1596±49	61±19	1.094
840	711.0±6.1	0.3341±0.0029	5928±88	96±15	1.356
820	329.0±3.0	0.3376±0.0022	5478±84	74±13	1.491
810.40	223.7±2.1	0.3384±0.0019	5989±86	27±5	1.463
809.79	67.8±0.8	0.3412±0.0012	1899±48	5±1	1.464
800.40	235.6±2.2	0.3399±0.0014	11694±121	40±10	1.319
799.79	53.6±0.7	0.3435±0.0013	2679±57	6±2	1.308
794.40	160.8±1.6	0.3408±0.0012	13757±129	19±4	1.165
793.79	54.8±0.7	0.3448±0.0010	5066±78	8±1	1.148
790.40	136.3±1.4	0.3414±0.0011	20228±157	15±4	1.036
789.79	58.8±0.7	0.3458±0.0010	9054±104	7±1	1.015
786.40	177.6±1.7	0.3420±0.0010	51265±251	27±5	0.895
786.18	20.4±0.4	0.3450±0.0037	6226±88	3±1	0.887
785.79	76.9±0.9	0.3466±0.0010	24876±175	10±1	0.874
785.40	222.4±2.1	0.3422±0.0010	75531±304	33±7	0.861
784.40	285.3±2.7	0.3424±0.0010	111828±371	34±5	0.830
783.79	78.1±0.9	0.3470±0.0010	33325±201	7±3	0.814
783.40	288.5±2.6	0.3424±0.0010	122114±387	80±10	0.804
782.90	122.3±1.2	0.3477±0.0012	54830±261	40±7	0.794
782.79	85.2±0.9	0.3473±0.0010	37956±217	16±3	0.792
782.40	300.9±2.7	0.3426±0.0010	127682±397	36±14	0.785
782.13	15.1±0.3	0.3534±0.0037	6452±89	4±2	0.781
781.79	372.5±3.3	0.3475±0.0010	155515±436	49±17	0.777
781.40	220.4±2.1	0.3427±0.0010	85611±324	85±10	0.773
780.40	169.2±1.6	0.3429±0.0010	56031±262	10±1	0.767
778.11	20.9±0.4	0.3534±0.0031	4344±72	8±4	0.767
780.79	131.9±1.3	0.3477±0.0010	48230±241	42±6	0.769
779.90	114.7±1.2	0.3457±0.0014	34860±207	14±5	0.766
779.79	44.7±0.6	0.3478±0.0010	13099±126	1±1	0.766
778.40	159.6±1.6	0.3432±0.0011	34568±207	21±3	0.767
777.79	79.2±0.9	0.3483±0.0010	14700±134	10±4	0.768
774.40	162.2±1.6	0.3439±0.0012	14157±131	21±6	0.779
773.79	65.1±0.8	0.3492±0.0010	4952±78	10±1	0.781
770.40	253.5±2.3	0.3445±0.0013	10959±116	33±7	0.792
769.79	45.9±0.6	0.3500±0.0011	1656±44	10±1	0.794
764.40	222.8±2.1	0.3455±0.0015	4242±71	31±7	0.806
763.79	40.2±0.6	0.3512±0.0013	724±30	5±1	0.808
760.40	208.2±2.0	0.3461±0.0017	2658±57	19±6	0.814
759.79	43.5±0.6	0.3520±0.0014	576±28	7±3	0.815
750.40	174.6±1.7	0.3479±0.0021	1008±37	26±7	0.826
749.79	52.2±0.7	0.3541±0.0018	251±18	14±5	0.828
720	584.1±5.0	0.3563±0.0069	652±30	60±8	0.848
690	174.4±1.6	0.3526±0.0069	58±11	21±5	0.860
660	281.1±2.5	0.3575±0.0070	40±11	29±4	0.862
630	120.1±1.2	0.3532±0.0068	0±5	14±3	0.865
600	90.6±0.9	0.3298±0.0066	−2±6	15±4	0.868
580	12.7±0.2	0.3561±0.0069	2±4	2±1	0.867
560	11.2±0.2	0.3369±0.0068	−1±1	1±1	0.867
540	12.1±0.2	0.3156±0.0067	−4±2	4±2	0.867
520	7.2±0.2	0.2866±0.0065	0	0	0.861
500	8.0±0.2	0.2278±0.0060	0±1	1±1	0.856
480	13.4±0.2	0.2030±0.0058	0	0	0.852
440	6.2±0.1	0.0183±0.0019	0	0	0.820

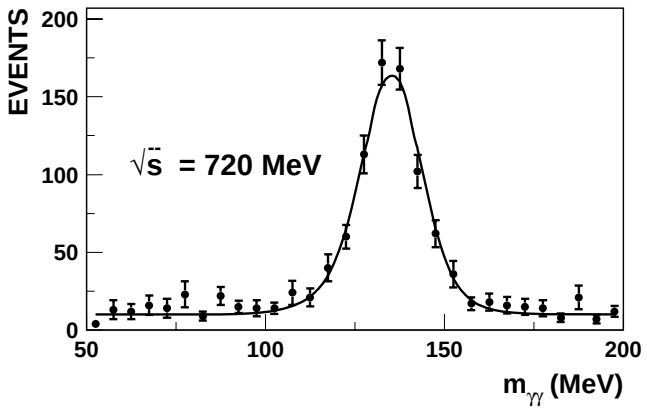

FIG. 13. The two-photon invariant mass distribution at $\sqrt{s}=720$ MeV.

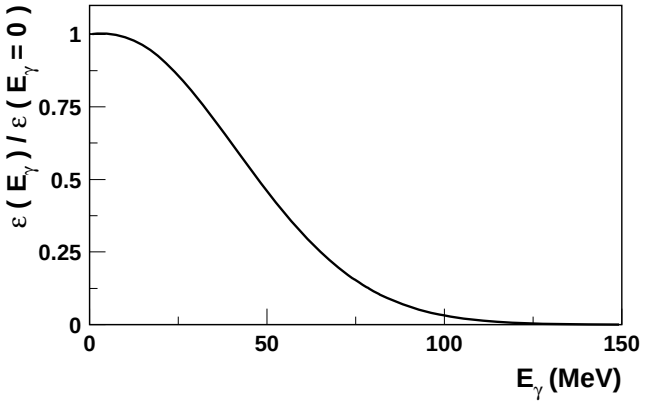

FIG. 14. The detection efficiency $\epsilon(E_\gamma)$ dependence on the radiated photon energy E_γ for the $e^+e^-\to\pi^+\pi^-\pi^0(\gamma)$ events at $\sqrt{s}\simeq m_\omega$, obtained by simulation.

detector was triggered by an external generator) were mixed with the simulated events. The detection efficiency for events without γ quantum radiation by the initial particles is about 0.35 (Table I). The detection efficiency dependence on the radiated photon energy is shown in Fig. 14. The efficiency decrease with the rise of the radiated photon energy is due to the selection criterion $\chi^2_{3\pi}<20$, which involves energy and momentum conservation in the $e^+e^-\to\pi^+\pi^-\pi^0$ process.

Inaccuracies in the simulation of the distributions over some selection parameters lead to an error in the determination of the average detection efficiency. To take these uncertainties into account, the detection efficiency was multiplied by correction coefficients, which were obtained in the following way [2,27]. The experimental events were selected without any conditions on the parameter under study, using selection parameters uncorrelated with the one studied. The same selection criteria were applied to simulated events. Then the cut was applied to the parameter and the correction coefficient was calculated:

$$\delta=\frac{n/N}{m/M}, \tag{2}$$

where N and M are the numbers of events in the experiment and simulations, respectively, selected without any cuts on the parameter under study; n and m are the numbers of events in the experiment and simulation when the cut on the parameter is applied. As a rule, the error in the coefficient δ determination is connected with the uncertainty of the background subtraction. This systematic error was estimated by varying other selection criteria.

The inaccuracy in the $\chi^2_{3\pi}$ distribution simulation (Fig. 2) is the main source of uncertainty in the detection efficiency determination. The correction coefficient $\delta_{\chi^2_{3\pi}}=0.95\pm0.02$ (Fig. 15) was obtained by using data collected in the vicinity of the ω resonance. The error due to uncertainty in the simulation of other parameters is estimated to be 1.7%. In the energy region $\sqrt{s}>900$ MeV the additional selection criterion $N_\gamma=2$ was applied. The uncertainty due to this cut was estimated to be 3%. The systematic error of the detection efficiency determination is 2.7% in the energy region $\sqrt{s}<900$ MeV and is about 4.1% at $\sqrt{s}>900$. The detection efficiency after the applied corrections is shown in Table I.

TABLE II. The ratio of the cross sections, obtained by using different methods of background subtraction. $N_{3\pi}$ is the number of $e^+e^-\to3\pi$ events obtained by fitting the two-photon invariant mass spectra. $\sigma(1)$ is the cross section measured in the approach when the background was calculated according to Eq. (1), $\sigma^{(2)}$ is the cross section measured by using the two-photon invariant mass spectra analysis.

$\sqrt{s}$ (MeV)	$N_{3\pi}$	$\sigma^{(1)}/\sigma^{(2)}$
750	1350 ± 42	0.995 ± 0.034
720	700 ± 32	0.999 ± 0.054
690	66 ± 11	0.956 ± 0.209
660	17 ± 10	2.562 ± 1.114

IV. THEORETICAL FRAMEWORK

In the framework of the vector meson dominance model, the cross section of the $e^+e^-\to\pi^+\pi^-\pi^0$ process is

$$\frac{d\sigma}{dm_0dm_+}=\frac{4\pi\alpha}{s^{3/2}}\frac{|\vec{p}_+\times\vec{p}_-|^2}{12\pi^2\sqrt{s}}m_0m_+\cdot|F|^2, \tag{3}$$

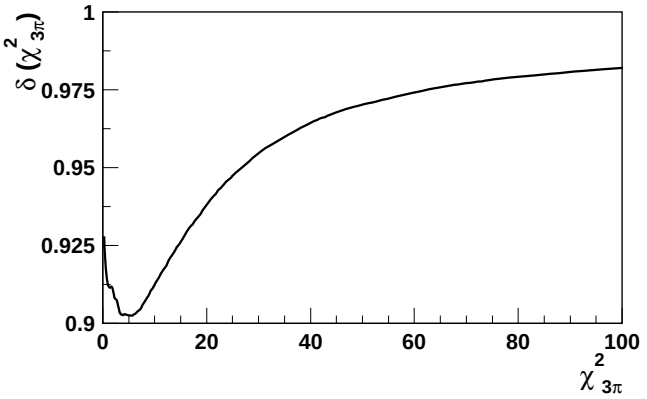

FIG. 15. The correction coefficient $\delta_{\chi^2_{3\pi}}$ dependence on the value of the cut on $\chi^2_{3\pi}$.

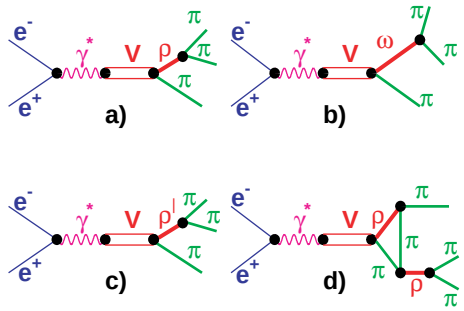

FIG. 16. The $e^+e^-\to\pi^+\pi^-\pi^0$ transition diagrams.

where $\vec{p}_+$ and $\vec{p}_-$ are the π^+ and π^- momenta, and m_0 and m_+ are the $\pi^+\pi^-$ and $\pi^+\pi^0$ pair invariant masses. The form factor F of the $\gamma^\star\to\pi^+\pi^-\pi^0$ transition has the form

$$|F|^2=\Bigg|A_{\rho\pi}(s)\sum_{i=+,0,-}\frac{g_{\rho^i\pi\pi}}{D_\rho(m_i)Z(m_i)}+A_{\rho'^{(\prime)}\pi}(s)\sum_{i=+,0,-}\frac{g_{\rho'^{(\prime)}\pi\pi}}{D_{\rho'^{(\prime)}}(m_i)}+A_{\omega\pi}(s)\frac{\Pi_{\rho\omega}g_{\rho^0\pi\pi}}{D_\rho(m_0)D_\omega(m_0)}\Bigg|^2. \tag{4}$$

The first term in Eq. (4) takes into account the $\gamma^\star\to\rho\pi\to\pi^+\pi^-\pi^0$ transition (Fig. 16a), which dominates in the process under study [28]. Here

$$D_\rho(m_i)=m_{\rho^i}^2-m_i^2-im_i\Gamma_{\rho^i}(m_i),$$

$$\Gamma_{\rho^i}(m_i)=\left(\frac{m_{\rho^i}}{m_i}\right)^2\Gamma_{\rho^i}\cdot\left(\frac{q_i(m_i)}{q_i(m_{\rho^i})}\right)^3,$$

$$q_0(m^2)=\frac{1}{2}(m^2-4m_\pi^2)^{1/2},$$

$$q_\pm(m^2)=\frac{1}{2m}\{[m^2-(m_{\pi^0}+m_\pi)^2][m^2-(m_{\pi^0}-m_\pi)^2]\}^{1/2},$$

$$m_-=\sqrt{s+m_{\pi^0}^2+2m_\pi^2-m_0^2-m_+^2},$$

where m_- is the $\pi^-\pi^0$ pair invariant mass, m_{π^0} and m_π are the neutral and charged pion masses, and i denotes the sign of the ρ meson ($\pi\pi$ pair) charge. The $\rho^0\to\pi^+\pi^-$ and $\rho^\pm\to\pi^\pm\pi^0$ transition coupling constants can be determined in the following way:

$$g_{\rho^0\pi\pi}^2=\frac{6\pi m_{\rho^0}^2\Gamma_{\rho^0}}{q_0(m_{\rho^0})^3},\quad g_{\rho^\pm\pi\pi}^2=\frac{6\pi m_{\rho^\pm}^2\Gamma_{\rho^\pm}}{q_\pm(m_{\rho^\pm})^3}.$$

Experimental data [28] do not contradict the equality of the coupling constants $g_{\rho^0\pi\pi}^2=g_{\rho^\pm\pi\pi}^2$. In this case the ρ^0 and $\rho^\pm$ meson widths are related as follows:

$$\Gamma_{\rho^\pm}=\Gamma_{\rho^0}\frac{m_{\rho^0}^2}{m_{\rho^\pm}^2}\frac{q_\pm(m_{\rho^\pm})^3}{q_0(m_{\rho^0})^3}. \tag{5}$$

In the subsequent analysis we assume that $g_{\rho^0\pi\pi}^2=g_{\rho^\pm\pi\pi}^2$, and the width values were taken from the SND measurements [28]: $\Gamma_{\rho^0}=149.8$ MeV, $\Gamma_{\rho^\pm}=150.9$ MeV. The neutral and charged ρ meson masses were assumed to be equal and were also taken from the SND measurements [28], $m_\rho=775.0$ MeV. The factor $Z(m)=1-is_1\Phi(m,s)$ takes into account the interaction of the ρ and π mesons in the final state [33] [Fig. 16(d)], and the parameter $s_1=1\pm0.2$ corresponds to the prediction of Ref. [33], where the concrete form of the $\Phi(m,s)$ function can be found. In experimental studies of the $\pi\pi$ mass spectra in the $e^+e^-\to3\pi$ process at $\sqrt{s}\simeq m_\phi$ [28], we obtained $s_1=0.3\pm0.3\pm0.3$. This result is consistent with zero, but also does not contradict the prediction of Ref. [33].

The second term in Eq. (4) takes into account the possible transition $\gamma^\star\to\rho'^{(\prime)}\pi\to\pi^+\pi^-\pi^0$ [Fig. 16(c)]. This term can be written as $A_{\rho\pi}(s)\cdot a_{3\pi}$, where

$$a_{3\pi}=\frac{A_{\rho'^{(\prime)}\pi}(s)}{A_{\rho\pi}(s)}\sum_{i=+,0,-}\frac{g_{\rho'^{(\prime)}\pi\pi}}{D_{\rho'^{(\prime)}}(m_i)}.$$

In the analysis, the $a_{3\pi}$ amplitude was assumed to be a real constant. From the $\pi\pi$ mass spectra analysis, in the process $e^+e^-\to3\pi$ at $\sqrt{s}\simeq m_\phi$ [28], it was found that $a_{3\pi}=(0.01\pm0.23\pm0.25)\times10^{-5}$ MeV^{-2}.

The third term in Eq. (4) takes into account the $\gamma^\star\to\omega\pi^0\to\pi^+\pi^-\pi^0$ transition [3] [Fig. 16(b)]. The polarization operator of the ρ-ω mixing satisfies $\mathrm{Im}(\Pi_{\rho\omega})\ll\mathrm{Re}(\Pi_{\rho\omega})$ [33,34], where

$$\mathrm{Re}(\Pi_{\rho\omega})=\sqrt{\frac{\Gamma_\omega}{\Gamma_{\rho^0}(m_\omega)}B(\omega\to\pi^+\pi^-)}\cdot|(m_\omega^2-m_\rho^2)-im_\omega[\Gamma_\omega-\Gamma_{\rho^0}(m_\omega)]|, \tag{6}$$

so we have assumed $\mathrm{Im}(\Pi_{\rho\omega})=0$ in the subsequent analysis.

The $e^+e^-\to\pi^+\pi^-\pi^0$ process cross section can be written in the following form:

$$\sigma_{3\pi}=\sigma_{\rho\pi\to3\pi}+\sigma_{\omega\pi\to3\pi}+\sigma_{int}, \tag{7}$$

where

$$\sigma_{\rho\pi\to3\pi}=\frac{4\pi\alpha}{s^{3/2}}W_{\rho\pi}(s)|A_{\rho\pi}(s)|^2, \tag{8}$$

$$\sigma_{\omega\pi\to3\pi}=\frac{4\pi\alpha}{s^{3/2}}W_{\omega\pi}(s)|A_{\omega\pi}(s)|^2, \tag{9}$$

$$\sigma_{int}=\frac{4\pi\alpha}{s^{3/2}}\{A_{\rho\pi}(s)A_{\omega\pi}^\star(s)W_{int}(s)+A_{\rho\pi}^\star(s)A_{\omega\pi}(s)W_{int}^\star(s)\}. \tag{10}$$

The phase space factors $W_{\rho\pi}(s)$, $W_{\omega\pi}(s)$, and $W_{int}(s)$ were calculated as follows:

$$W_{\rho\pi}(s)=\frac{1}{12\pi^2\sqrt{s}}\int_{2m_\pi}^{\sqrt{s}-m_{\pi^0}} m_0 dm_0 \int_{m_+^{min}(m_0)}^{m_+^{max}(m_0)} m_+ dm_+ |\vec{p}_+ \times \vec{p}_-|^2 \cdot \left| \sum_{i=+,0,-} \frac{g_{\rho^i\pi\pi}}{D_\rho(m_i)Z(m_i)} + a_{3\pi} \right|^2, \quad (11)$$

$$W_{\omega\pi}(s)=\frac{1}{12\pi^2\sqrt{s}}\int_{2m_\pi}^{\sqrt{s}-m_{\pi^0}} m_0 dm_0 \int_{m_+^{min}(m_0)}^{m_+^{max}(m_0)} m_+ dm_+ |\vec{p}_+ \times \vec{p}_-|^2 \cdot \left| \frac{\Pi_{\rho\omega} g_{\rho^0\pi\pi}}{D_\rho(m_0)D_\omega(m_0)} \right|^2, \quad (12)$$

$$W_{int}(s)=\frac{1}{12\pi^2\sqrt{s}}\int_{2m_\pi}^{\sqrt{s}-m_{\pi^0}} m_0 dm_0 \int_{m_+^{min}(m_0)}^{m_+^{max}(m_0)} m_+ dm_+ |\vec{p}_+ \times \vec{p}_-|^2 \left[\frac{\Pi_{\rho\omega} g_{\rho^0\pi\pi}}{D_\rho(m_0)D_\omega(m_0)} \right]^\star \times \left[\sum_{i=+,0,-} \frac{g_{\rho^i\pi\pi}}{D_\rho(m_i)Z(m_i)} + a_{3\pi} \right]. \quad (13)$$

The amplitudes of the $\gamma^\star \to \rho\pi$ transition have the form

$$A_{\rho\pi}(s)=\frac{1}{\sqrt{4\pi\alpha}} \sum_{V=\omega,\rho,\phi,\omega',\omega''} \frac{\Gamma_V m_V^2 \sqrt{m_V \sigma(V\to 3\pi)}}{D_V(s)} \times \frac{e^{i\phi_{\omega V}} C_{V\rho\pi}(s,r_0)}{\sqrt{W_{\rho\pi}(m_V)}}, \quad (14)$$

where

$$D_V(s)=m_V^2 - s - i\sqrt{s}\Gamma_V(s), \quad \Gamma_V(s)=\sum_f \Gamma(V\to f,s).$$

Here f denotes the final state of the vector meson V decay, m_V is the vector meson mass, and $\Gamma_V=\Gamma_V(m_V)$. The ϕ meson mass and width were taken from the SND measurements $m_\phi=1019.42$ MeV, $\Gamma_\phi=4.21$ MeV [27]. The following forms of the energy dependence of the vector meson total widths were used:

$$\Gamma_\rho(s)=\frac{m_\rho^2}{s}\frac{q_0(s)^3}{q_0(m_\rho)^3}\Gamma_\rho C_{\rho\pi\pi}^2(s,r_0)+\frac{g_{\rho\omega\pi}^2}{12\pi}q_{\omega\pi}^3(s),$$

$$\Gamma_\omega(s)=\frac{m_\omega^2}{s}\frac{q_0(s)^3}{q_0(m_\omega)^3}\Gamma_\omega B(\omega\to\pi^+\pi^-) C_{\omega\pi\pi}^2(s,r_0) + \frac{q_{\pi\gamma}(s)^3}{q_{\pi\gamma}(m_\omega)^3}\Gamma_\omega B(\omega\to\pi^0\gamma) C_{\omega\gamma\pi}^2(s,r_0) + \frac{W_{\rho\pi}(s)}{W_{\rho\pi}(m_\omega)}\Gamma_\omega B(\omega\to 3\pi) C_{\omega\rho\pi}^2(s,r_0),$$

$$\Gamma_\phi(s)=\frac{m_\phi^2}{s}\frac{q_{K^\pm}(s)^3}{q_{K^\pm}(m_\phi)^3}\Gamma_\phi B(\phi\to K^+K^-) C_{\phi K^+K^-}^2(s,r_0) + \frac{m_\phi^2}{s}\frac{q_{K^0}(s)^3}{q_{K^0}(m_\phi)^3}\Gamma_\phi B(\phi\to K_S K_L) C_{\phi K_S K_L}^2(s,r_0) + \frac{q_{\eta\gamma}(s)^3}{q_{\eta\gamma}(m_\phi)^3}\Gamma_\phi B(\phi\to\eta\gamma) C_{\phi\gamma\eta}^2(s,r_0) + \frac{W_{\rho\pi}(s)}{W_{\rho\pi}(m_\phi)}\Gamma_\phi B(\phi\to 3\pi) C_{\phi\rho\pi}^2(s,r_0),$$

$$\Gamma_{\omega'}(s)=\Gamma_{\omega'} C_{\omega'\rho\pi}^2(s,r_0)\frac{W_{\rho\pi}(s)}{W_{\rho\pi}(m_{\omega'})},$$

$$\Gamma_{\omega''}(s)=\Gamma_{\omega''} C_{\omega''\rho\pi}^2(s,r_0)\left(\frac{W_{\rho\pi}(s)}{W_{\rho\pi}(m_{\omega''})} B(\omega''\to 3\pi) + \frac{W_{\omega\pi\pi}(s)}{W_{\omega\pi\pi}(m_{\omega''})} B(\omega''\to\omega\pi\pi) \right).$$

Here $g_{\rho\omega\pi}$ is the coupling constant of the $\rho\to\omega\pi^0$ transition, $q_{\omega\pi}$, $q_{K^\pm}$, q_{K^0}, $q_{\pi\gamma}$, and $q_{\eta\gamma}$ are the ω meson, kaon, η meson, and pion momenta, $W_{\omega\pi\pi}(s)$ is the phase space factor of the $\omega\pi\pi$ final state [35], and $C_{VPP}(s,r_0)$ and $C_{VVP}(s,r_0)$ are the form factors which restrict too fast growth with the energy of the partial widths, so that $\sqrt{s}\Gamma(s)\to$const as $s\to\infty$. According to Ref. [36] these form factors can be written as follows:

$$C_{V\gamma(\rho)P}(s,r_0)=\frac{1+(r_0 m_V)^2}{1+(r_0\sqrt{s})^2},$$

$$C_{VPP}(s,r_0)=\sqrt{\frac{1+[r_0 q_P(m_V)]^2}{1+[r_0 q_P(s)]^2}}, \quad (15)$$

where q_P is the momentum of the pseudoscalar meson and r_0 is the range parameter (its value was taken to be the same for all decays).

The relative probabilities of the decays were calculated as follows:

$$B(V\to X)=\frac{\sigma(V\to X)}{\sigma(V)}, \quad \sigma(V)=\sum_X \sigma(V\to X),$$

$$\sigma(V\to X)=\frac{12\pi B(V\to e^+e^-)B(V\to X)}{m_V^2}.$$

In particular,

$$B(\omega\to X)=\frac{\sigma(\omega\to X)}{\sigma(\omega)},$$

$$\sigma(\omega)=\frac{\sigma(\omega\to 3\pi)+\sigma(\omega\to\pi^0\gamma)}{1-B(\omega\to\pi^+\pi^-)}.$$

In further analysis we have used $\sigma(\omega\to\pi^0\gamma)=155.8$ nb, $\sigma(\phi\to K^+K^-)=1968$ nb, $\sigma(\phi\to K_SK_L)=1451$ nb, and $\sigma(\phi\to\eta\gamma)=54.8$ nb obtained in the SND experiments [27,37,38].

$\phi_{\omega V}$ is the relative interference phase between the vector meson V and ω, so $\phi_{\omega\omega}=0°$. The phases $\phi_{\omega V}$ can deviate from 0° or 180° and their values can be energy dependent due to mixing between vector mesons. For example, the phase $\phi_{\omega\phi}$ was found to be close to 180° [2,27] in agreement with the prediction [39] $\phi_{\omega\phi}=\Phi(s)$ [$\Phi(m_\phi)\simeq 163°$], where the function $\Phi(s)$ is defined in Ref. [39]. In Ref. [2] it was shown that $\phi_{\omega\omega'}\sim 180°$ and $\phi_{\omega\omega''}\sim 0°$, so in this work these two phases were fixed at those values.

Taking into account the ρ-ω mixing, the $\omega\to\rho\pi$ and $\rho\to\rho\pi$ transition amplitudes can be written in the following way [3,34]:

$$A_{\omega\to\rho\pi}+A_{\rho\to\rho\pi}=\frac{g^{(0)}_{\gamma\omega}g^{(0)}_{\omega\rho\pi}}{D_\omega(s)}\left[1+\frac{g^{(0)}_{\gamma\rho}}{g^{(0)}_{\gamma\omega}}\varepsilon(s)\right]+\frac{g^{(0)}_{\gamma\rho}g^{(0)}_{\omega\rho\pi}}{D_\rho(s)}\left[\frac{g^{(0)}_{\rho\rho\pi}}{g^{(0)}_{\omega\rho\pi}}-\varepsilon(s)\right],\quad(16)$$

where

$$\varepsilon(s)=\frac{-\Pi_{\rho\omega}}{D_\omega(s)-D_\rho(s)},$$

$$|g_{V\gamma}|=\left[\frac{3m_V^3\Gamma_V B(V\to e^+e^-)}{4\pi\alpha}\right]^{1/2},$$

$$|g_{V\rho\pi}|=\left[\frac{4\pi\Gamma_V B(V\to\rho\pi)}{W_{\rho\pi}(m_V)}\right]^{1/2}.$$

The superscript (0) denotes the coupling constants of the pure, unmixed state. Equation (16) can be rewritten as follows:

$$A_{\omega\to\rho\pi}+A_{\rho\to\rho\pi}=\frac{1}{\sqrt{4\pi\alpha}}\sum_{V=\omega,\rho}\frac{\Gamma_V m_V^2\sqrt{m_V\sigma(V\to 3\pi)}}{D_V(s)}\times\frac{f_{V\rho\pi}(s)C_{V\rho\pi}(s,r_0)}{\sqrt{W_{\rho\pi}(m_V)}},$$

where

$$f_{V\rho\pi}(s)=\frac{r_{V\rho\pi}(s)}{r_{V\rho\pi}(m_V)},$$

$$r_{\omega\rho\pi}(s)=1+\frac{g^{(0)}_{\gamma\rho}}{g^{(0)}_{\gamma\omega}}\varepsilon(s)\simeq 1+\left[\frac{m_\rho^3\Gamma(\rho\to e^+e^-)}{m_\omega^3\Gamma(\omega\to e^+e^-)}\right]^{1/2}\varepsilon(s),$$

$$r_{\rho\rho\pi}(s)=\frac{g^{(0)}_{\rho\rho\pi}}{g^{(0)}_{\omega\rho\pi}}-\varepsilon(s)\simeq-\varepsilon(s).$$

If the $\rho\to 3\pi$ transition proceeds only via ρ-ω mixing, that is, $g^{(0)}_{\rho\rho\pi}=0$, then $\phi_{\omega\rho}\simeq -90°$ and almost does not depend on energy; in addition,

$$\sigma(\rho\to 3\pi)\simeq\sigma(\omega\to 3\pi)\frac{m_\omega^2}{m_\rho^2}\frac{\Gamma_\omega}{\Gamma_\rho}\frac{W_{\rho\pi}(m_\rho)}{W_{\rho\pi}(m_\omega)}\times\frac{r_{\rho\rho\pi}(m_\rho)}{r_{\omega\rho\pi}(m_\omega)}\frac{B(\rho\to e^+e^-)}{B(\omega\to e^+e^-)}.$$

For the $\gamma^\star\to\omega\pi^0$ transition amplitude, a model that gives a satisfactory description of the relative phase between it and the $A_{\rho\pi}(s)$, Eq. (14), amplitude [2] was used:

$$A_{\omega\pi}(s)=\sqrt{\frac{3}{4\pi\alpha}}\times\left[\frac{\sqrt{m_\rho^3\Gamma_\rho B(\rho\to e^+e^-)}g_{\rho\omega\pi}}{D_\rho(s)}+\sum_{V=\rho',\rho''}\frac{\Gamma_V m_V^2\sqrt{m_V\sigma(V\to\omega\pi^0)}}{D_V(s)}\frac{e^{i\phi_{\rho V}}}{\sqrt{q^3_{\omega\pi}(m_V)}}\right],\quad(17)$$

where $\phi_{\rho\rho}=0°$, $m_{\rho'}=1480$ MeV, $\Gamma_{\rho'}=790$ MeV, $\sigma(\rho'\to\omega\pi^0)=86$ nb, $\phi_{\rho'}=180°$, $m_{\rho''}=1640$ MeV, $\Gamma_{\rho''}=1290$ MeV, $\sigma(\rho''\to\omega\pi^0)=48$ nb, $\phi_{\rho'}=0°$, $g_{\rho\omega\pi}=16{,}8$ GeV^{-1}, and

$$\Gamma_{\rho'(\prime\prime)}(s)=\Gamma_{\rho'(\prime\prime)}\frac{q^3_{\omega\pi}(s)}{q^3_{\omega\pi}(m_V)}.$$

V. CROSS SECTION MEASUREMENT

From the data in Table I, the cross section of the process $e^+e^-\to\pi^+\pi^-\pi^0$ can be calculated as follows:

$$\sigma(s)=\frac{N_{3\pi}(s)}{\mathcal{L}(s)\xi(s)},\quad(18)$$

where $N_{3\pi}(s)$ is the number of selected $e^+e^-\to\pi^+\pi^-\pi^0(\gamma)$ events, $\mathcal{L}(s)$ is the integrated luminosity, $\xi(s)$ is a function that takes into account the detection efficiency and radiative corrections for the initial state radiation:

$$\xi(s)=\frac{\int_0^{E_\gamma^{max}}\sigma_{3\pi}(s,E_\gamma)F(s,E_\gamma)\epsilon(s,E_\gamma)dE_\gamma}{\sigma_{3\pi}(s)}.\quad(19)$$

Here E_γ is the emitted photon energy, $F(s,E_\gamma)$ is the electron "radiator" function [40], $\epsilon(s,E_\gamma)$ is the detection efficiency of the process $e^+e^-\to\pi^+\pi^-\pi^0(\gamma_{rad})$ as a function of the emitted photon energy and the total energy in the e^+e^- center of mass system, and $\sigma_{3\pi}(s)$ is the theoretical energy dependence of the cross section given by Eq. (7).

To obtain the values of $\xi(s)$ at each energy point, the visible cross section of the process $e^+e^-\to\pi^+\pi^-\pi^0(\gamma_{rad})$

$$\sigma^{vis}(s)=\frac{N_{3\pi}(s)}{\mathcal{L}(s)}$$

was fitted by the theoretical energy dependence

$$\sigma^{th}(s)=\sigma_{3\pi}(s)\xi(s).$$

The following logarithmic likelihood function was minimized:

$$\chi^2=\sum_i \frac{(\sigma_i^{vis}-\sigma_i^{th})^2}{\Delta_i^2},$$

where i is the energy point number and Δ_i is the error of the visible cross section σ^{vis}.

In the fit the ϕ,ω',ω'' meson parameters (the mass, width, and branching ratios of the main decays) were fixed at their values obtained in the SND experiments [2,27]; other parameters were fixed as follows: $r_0=0$, $a_{3\pi}=0$, $s_1=0$, and $\phi_{\omega\phi}=\Phi(s)$ $[\Phi(m_\phi)\simeq 163°]$. Equation (14) was written in the following form:

$$A_{\rho\pi}(s)=\frac{1}{\sqrt{4\pi\alpha}}\sum_{V=\omega,\rho,\phi,\omega',\omega''}\frac{\Gamma_V m_V^2\sqrt{m_V\sigma(V\to 3\pi)}}{D_V(s)}\times\frac{e^{i\phi_{\omega V}}}{\sqrt{W_{\rho\pi}(m_V)}}+C_{3\pi}, \tag{20}$$

where $C_{3\pi}$ is a complex constant.

$\sigma(\omega\to 3\pi)$, Γ_ω, and m_ω were the free parameters of the fit. The $\xi(s)$ values were obtained from approximation of the experimental data in several models: (1) $\sigma(\rho\to 3\pi)=0$, $C_{3\pi}=0$; (2) $\sigma(\rho\to 3\pi)$ and $\phi_{\omega\rho}$ are free parameters, $C_{3\pi}=0$; (3) $C_{3\pi}$ is a free parameter, $\sigma(\rho\to 3\pi)=0$; (4) $\sigma(\rho\to 3\pi)$, $\phi_{\omega\rho}$, and $C_{3\pi}$ are free parameters. The fits were also performed under the same assumptions, but with $\sigma(\omega'\to 3\pi)=0$ and $\sigma(\omega''\to 3\pi)=0$.

The values of $\xi(s)$ actually do not depend on the applied model. The largest model dependence, about 1.5–2 %, was found at $\sqrt{s}$ from 800 to 840 MeV. Using the obtained $\xi(s)$ values, the cross section of the $e^+e^-\to\pi^+\pi^-\pi^0$ process was calculated (Table III). The systematic error of the cross section determination at each energy point $\sqrt{s}$ is equal to

$$\sigma_{sys}=\sigma_{eff}\oplus\sigma_{\mathcal{L}}\oplus\sigma_{mod}(s)\oplus\sigma_{bkg}(s).$$

Here $\sigma_{eff}=2.7\%$ at $\sqrt{s}<900$ MeV and $\sigma_{eff}=4.1\%$ at $\sqrt{s}>900$ MeV, $\sigma_{\mathcal{L}}=2\%$. They are systematic uncertainties in the detection efficiency and integrated luminosity, which are common for all energy points. The model uncertainty $\sigma_{mod}(s)$ was obtained from the difference between the $\xi(s)$ values determined for the models mentioned above. The error $\sigma_{bkg}(s)$ takes into account the inaccuracy ($\sim 60\%$) of the background subtraction and depends on the beam energy.

VI. THE $e^+e^-\to\pi^+\pi^-\pi^0$ CROSS SECTION ANALYSIS

The cross section measured in this work (Table III) was analyzed together with the $e^+e^-\to\pi^+\pi^-\pi^0$ cross section measured by SND in the energy region $\sqrt{s}$ from 980 up to 1380 MeV [2,27] and with the DM2 results for the $e^+e^-\to\pi^+\pi^-\pi^0$ and $e^+e^-\to\omega\pi^+\pi^-$ cross section measurements in the energy region $\sqrt{s}$ from 1340 to 2200 MeV [25].

The $e^+e^-\to\pi^+\pi^-\pi^0$ cross section was fitted by the expression (7). The $e^+e^-\to\omega\pi^+\pi^-$ process cross section was written in the following way:

$$\sigma_{\omega\pi\pi}=\frac{1}{s^{3/2}}\left|\frac{\Gamma_{\omega''}m_{\omega''}^2\sqrt{\sigma(\omega''\to\omega\pi^+\pi^-)m_{\omega''}}}{D_{\omega''(s)}}\times\sqrt{\frac{W_{\omega\pi\pi}(s)C_{VVP}(s,r_0)}{W_{\omega\pi\pi}(m_{\omega''})}}\right|^2. \tag{21}$$

Here we have neglected the $\omega'\to\omega\pi\pi$ contribution. To calculate $B(\omega''\to\omega\pi\pi)$, we have assumed $\sigma(\omega''\to\omega\pi\pi)=1.5\cdot\sigma(\omega''\to\omega\pi^+\pi^-)$.

The cross sections of the $e^+e^-\to\pi^+\pi^-\pi^0$ and $\omega\pi^+\pi^-$ processes, measured by SND and DM2, were fitted together. The function to be minimized was

$$\chi^2_{tot}=\chi^2_{3\pi(SND)}+\chi^2_{3\pi(DM2)}+\chi^2_{\omega\pi\pi(DM2)},$$

where

$$\chi^2_{3\pi(SND)}=\sum_s\left(\frac{\sigma_{3\pi}^{(SND)}(s)-\sigma_{3\pi}(s)}{\Delta_{3\pi}^{(SND)}(s)}\right)^2,$$

$$\chi^2_{3\pi(DM2)}=\sum_s\left(\frac{C\cdot\sigma_{3\pi}^{(DM2)}(s)-\sigma_{3\pi}(s)}{\Delta_{3\pi}^{(DM2)}(s)}\right)^2,$$

$$\chi^2_{\omega\pi\pi(DM2)}=\sum_s\left(\frac{C\cdot\sigma_{\omega\pi\pi}^{(DM2)}(s)-\sigma_{\omega\pi\pi}(s)}{\Delta_{\omega\pi\pi}^{(DM2)}(s)}\right)^2.$$

Here $\sigma_{3\pi(\omega\pi\pi)}^{[SND(DM2)]}(s)$ are the experimental cross sections, Δ are their uncertainties, and C is a coefficient which take into account the relative systematic bias between SND and DM2 data. The errors $\Delta_{3\pi}^{(SND)}$ include both the statistical σ_{stat} and the systematic errors: $\Delta_{3\pi}^{(SND)}=\sigma_{stat}\oplus\sigma_{mod}\oplus\sigma_{bkg}$. The relative systematic bias between the SND and DM2 data was analyzed in Ref. [2] and the C coefficient was estimated to be $C=1.54$. In the analysis that follows we have fixed this coefficient at 1 or 1.54.

In the fittings m_ω, Γ_ω, $\sigma(\omega\to 3\pi)$, $\sigma(\phi\to 3\pi)$, $\phi_{\omega\phi}$, $m_{\omega'}$, $\Gamma_{\omega'}$, $\sigma(\omega'\to 3\pi)$, $m_{\omega''}$, $\Gamma_{\omega''}$, $\sigma(\omega''\to 3\pi)$, and $\sigma(\omega''\to\omega\pi^+\pi^-)$ were the free parameters. The approximations were performed under the following assumptions about the phase space factor for the $\pi^+\pi^-\pi^0$ final state: (1) $s_1=0$, $a_{3\pi}=0$; (2) $s_1=1$, $a_{3\pi}=0$; (3) $s_1=0$, $a_{3\pi}=-4\times 10^{-6}$ MeV^{-2}; (4) $s_1=0$, $a_{3\pi}=4\times 10^{-6}$ MeV^{-2}.

The nonzero values of the $a_{3\pi}$ amplitude are the upper limits imposed on the 90% confidence level by using the SND result reported in Ref. [28]. The approximations were also performed without taking into account the contribution from the $e^+e^-\to\omega\pi^0\to\pi^+\pi^-\pi^0$ process, i.e., by assuming $\sigma_{3\pi}=\sigma_{\rho\pi}$. The difference in the fit results was included in the model uncertainty.

The fittings were performed using the following model parameters: (1) $r_0=0$, $\sigma(\rho\to 3\pi)=0$; (2) $r_0=0$, $\phi_{\omega\rho}$ and $\sigma(\rho\to 3\pi)$ are free parameters; (3) $\sigma(\rho\to 3\pi)=0$, r_0 is a free parameter.

TABLE III. The $e^+e^- \to \pi^+\pi^-\pi^0$ cross section. σ_{mod} is the model uncertainty, σ_{bkg} is the error due to background subtraction, $\sigma_{eff} \oplus \sigma_{\mathcal{L}}$ is the error due to uncertainty in the detection efficiency and integrated luminosity determination (3.4% at $\sqrt{s} < 900$ MeV and 4.5% for $\sqrt{s} > 900$ MeV), and $\sigma_{sys} = \sigma_{eff} \oplus \sigma_{\mathcal{L}} \oplus \sigma_{mod}(s) \oplus \sigma_{bkg}(s)$ is the total systematic error.

$\sqrt{s}$ (MeV)	σ (nb)	σ_{bkg} (nb)	σ_{mod} (nb)	$\sigma_{eff} \oplus \sigma_{\mathcal{L}}$ (nb)	σ_{sys} (nb)
970.00	12.82 ± 0.70	0.32	0.05	0.58	0.66
958.00	11.33 ± 0.64	0.28	0.05	0.51	0.58
950.00	11.17 ± 0.62	0.29	0.06	0.50	0.58
940.00	9.83 ± 0.41	0.26	0.05	0.44	0.52
920.00	9.82 ± 0.39	0.24	0.04	0.44	0.50
880.00	11.22 ± 0.36	0.26	0.03	0.38	0.46
840.00	18.77 ± 0.33	0.18	0.21	0.64	0.70
820.00	32.93 ± 0.58	0.27	0.34	1.12	1.20
810.40	53.84 ± 1.01	0.15	0.41	1.83	1.88
809.79	55.81 ± 1.60	0.09	0.42	1.90	1.95
800.40	110.42 ± 1.82	0.23	0.42	3.75	3.78
799.79	111.09 ± 2.98	0.15	0.41	3.78	3.80
794.40	215.25 ± 3.91	0.18	0.31	7.32	7.33
793.79	233.54 ± 5.48	0.22	0.32	7.94	7.95
790.40	419.31 ± 8.24	0.19	0.56	14.26	14.27
789.79	437.91 ± 10.55	0.20	0.37	14.89	14.89
786.40	943.63 ± 19.81	0.30	1.45	32.08	32.12
786.18	998.92 ± 24.90	0.29	0.61	33.96	33.97
785.79	1068.39 ± 23.36	0.26	0.86	36.33	36.34
785.40	1154.29 ± 22.45	0.30	1.91	39.25	39.29
784.40	1382.69 ± 21.80	0.25	2.44	47.01	47.08
783.79	1514.97 ± 22.99	0.19	0.74	51.51	51.51
783.40	1542.58 ± 17.29	0.61	2.16	52.45	52.50
782.90	1627.56 ± 18.88	0.71	0.32	55.34	55.34
782.79	1624.77 ± 20.43	0.41	0.47	55.24	55.25
782.40	1584.21 ± 17.63	0.27	2.59	53.86	53.93
782.13	1552.85 ± 40.68	0.58	0.46	52.80	52.80
781.79	1550.80 ± 21.87	0.29	0.44	52.73	52.73
781.40	1470.94 ± 25.52	0.88	2.49	50.01	50.08
780.79	1369.11 ± 28.77	0.72	0.51	46.55	46.56
780.40	1261.06 ± 28.76	0.14	2.18	42.88	42.93
779.90	1146.89 ± 28.79	0.28	0.43	38.99	39.00
779.79	1098.85 ± 30.58	0.05	0.40	37.36	37.36
778.40	822.81 ± 21.45	0.30	1.52	27.98	28.02
778.11	765.41 ± 20.01	0.85	0.23	26.02	26.04
777.79	693.08 ± 19.36	0.28	0.23	23.56	23.57
774.40	325.90 ± 7.86	0.29	0.69	11.08	11.11
773.79	278.72 ± 7.87	0.34	0.08	9.48	9.48
770.40	158.58 ± 3.36	0.29	0.37	5.39	5.41
769.79	129.74 ± 4.55	0.47	0.06	4.41	4.44
764.40	68.48 ± 1.58	0.30	0.26	2.33	2.36
763.79	63.43 ± 2.87	0.26	0.06	2.16	2.17
760.40	45.38 ± 1.18	0.19	0.13	1.54	1.56
759.79	46.14 ± 2.34	0.34	0.06	1.57	1.61
750.40	20.12 ± 0.78	0.31	0.08	0.68	0.76
749.79	16.40 ± 1.22	0.55	0.04	0.56	0.78
720.00	3.69 ± 0.19	0.20	0.01	0.13	0.24
690.00	1.10 ± 0.21	0.24	0.00	0.04	0.24
660.00	0.46 ± 0.13	0.20	0.00	0.02	0.20
630.0	< 0.34 (90% C.L.)				
600.0	< 0.53 (90% C.L.)				
580.0	< 1.36 (90% C.L.)				
560.0	< 0.44 (90% C.L.)				
540.0	< 1.21 (90% C.L.)				
520.0	< 1.3 (90% C.L.)				
500.0	< 0.96 (90% C.L.)				
480.0	< 0.99 (90% C.L.)				
440.0	< 24.7 (90% C.L.)				

TABLE IV. Fit results for the $e^+e^-\to\pi^+\pi^-\pi^0$ and $\omega\pi^+\pi^-$ cross sections. The column number N corresponds to the different models for the $A_{\rho\pi}$ amplitude. N_{fit} is the number of fitted points. The first error is statistical; the second error shows the difference in the fit results due to various assumptions about the $e^+e^-\to\pi^+\pi^-\pi^0$ reaction dynamics and the relative systematics between the SND and DM2 measurements.

	N		
	1	2	3
m_ω (MeV)	782.75 ± 0.08	782.72 ± 0.08	782.71 ± 0.08
Γ_ω (MeV)	$8.60\pm0.04\pm0.01$	$8.73\pm0.04\pm0.02$	8.63 ± 0.04
$\sigma(\omega\to3\pi)$ (nb)	$1609\pm7\pm1$	$1624\pm10\pm5$	$1610\pm7\pm3$
$\sigma(\phi\to3\pi)$ (nb)	$645\pm6\pm4$	$645\pm7\pm6$	$658\pm8\pm7$
$\phi_{\omega\phi}$ (deg)	$161\pm2\pm4$	$163^{+3}_{-2}\pm4$	$187\pm4\pm6$
r_0 (GeV^{-1})			$2.6^{+1.1}_{-0.8}\pm0.2$
$m_{\omega'}$ (MeV)	$1358\pm20\pm45$	$1460^{+70}_{-50}\pm70$	$1410\pm30\pm60$
$\Gamma_{\omega'}$ (MeV)	$500^{+60}_{-50}\pm80$	$1120^{+500}_{-300}\pm200$	$617\pm40\pm95$
$\sigma(\omega'\to3\pi)$ (nb)	$5.7^{+0.4}_{-0.3}\pm0.5$	$3.7\pm0.7\pm0.4$	$5.0\pm0.2\pm0.4$
$m_{\omega''}$ (MeV)	$1808^{+60}_{-40}\pm20$	$1760\pm50\pm40$	$1750\pm20\pm6$
$\Gamma_{\omega''}$ (MeV)	$807^{+500}_{-200}\pm213$	$540^{+200}_{-100}\pm50$	$373\pm50\pm15$
$\sigma(\omega''\to3\pi)$ (nb)	$1.48\pm0.40\pm0.46$	$2.4\pm0.7\pm0.9$	$2.7\pm0.4\pm1.3$
$\sigma(\omega''\to\omega\pi^+\pi^-)$ (nb)	$1.54\pm0.30\pm0.45$	$1.8\pm0.4\pm0.5$	$2.2\pm0.3\pm0.4$
$\sigma(\rho\to3\pi)$ (nb)		$0.13^{+0.06}_{-0.04}\pm0.02$	
$\phi_{\omega\rho}$ (deg)		$-137^{+14}_{-10}\pm7$	
χ^2_ω/N_{fit}	(80–120)/49	(56–62)/49	(45–50)/49
$\chi^2_{(1)}/N_{fit}$	(21–46)/6	(13.6–16.4)/6	(7.3–11.3)/6
$\chi^2_{(SND)}/N_{fit}$	(66–92)/67	(49–56)/67	(58–67)/67
$\chi^2_{3\pi(DM2)}/N_{fit}$	(22–37)/18	(22–44)/18	(27–42)/18
$\chi^2_{\omega\pi\pi(DM2)}/N$	(11–15)/18	10/18	(23–26)/18
χ^2_{tot}/N_{fit}	(182–260)/152	(137–170)/152	(156–180)/152

The results of the fits are shown in Table IV and in Figs. 17–22. In Table IV, χ^2_ω, $\chi^2_{(SND)}$ ($\chi^2_{3\pi(SND)}=\chi^2_\omega+\chi^2_{(SND)}$), and $\chi^2_{(1)}$ denote the χ^2 values for the energy regions $\sqrt{s}$ below and above 970 MeV and in the energy range $880\leqslant\sqrt{s}\leqslant970$ MeV. The χ^2 values in the first model (column 1 in Table IV) are too large and this model contradicts the experimental data. The second and third models (columns 2 and 3 in Table IV) are in agreement with the experimental data. The χ^2_{tot} value for the second model is less than for the third one. If $\sigma(\rho\to3\pi)$, $\phi_{\omega\rho}$, and r_0 are the free parameters in the fit, then they are found to be equal to $\sigma(\rho\to3\pi)=0.11^{+0.06}_{-0.04}$ nb, $\phi_{\omega\rho}=-136^{+12\circ}_{-10^\circ}$, and $r_0=0.2\pm0.3$ GeV^{-1}. In this case the value of the range parameter r_0 turns out to be rather small and consistent with zero. The value of χ^2_{SND} for the second model is less than for the third one, and vice versa the χ^2_ω for the third model is less than for the second.

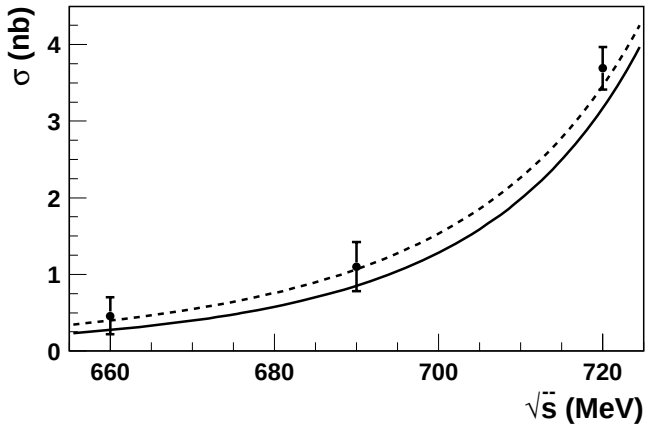

FIG. 17. The $e^+e^-\to\pi^+\pi^-\pi^0$ cross section. Dots are the SND data obtained in this work. Curves are results of fitting to the data in model 2 (solid curve) and in model 3 (dashed curve).

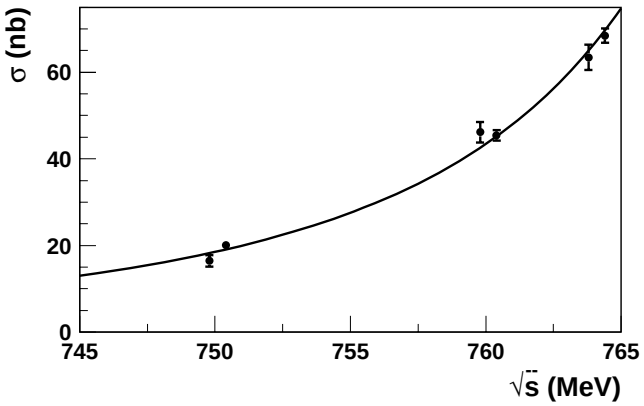

FIG. 18. The $e^+e^-\to\pi^+\pi^-\pi^0$ cross section. Dots are the SND data obtained in this work; the curve is the fit result.

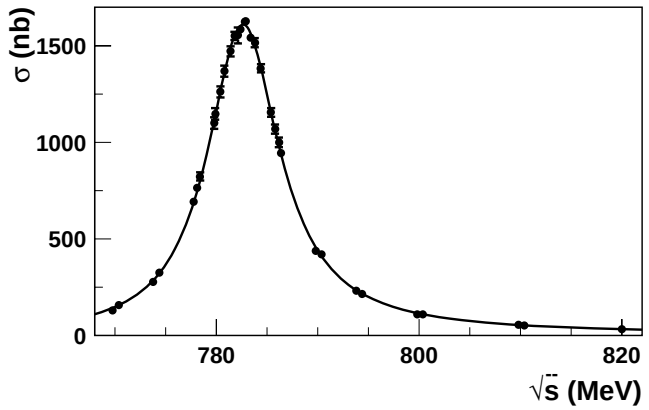

FIG. 19. The $e^+e^-\to\pi^+\pi^-\pi^0$ cross section. Dots are the SND data obtained in this work; the curve is the fit result.

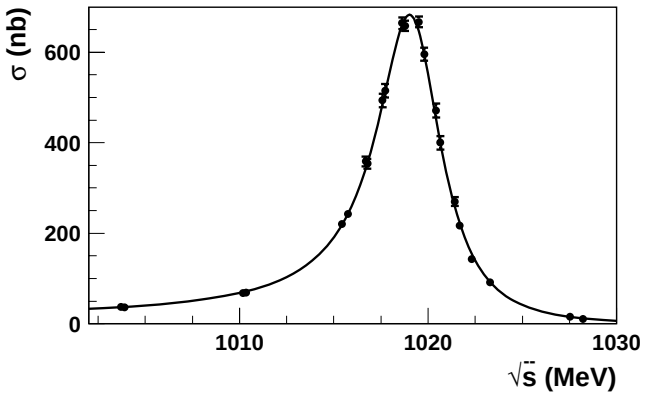

FIG. 21. The $e^+e^-\to\pi^+\pi^-\pi^0$ cross section. Dots are the SND data obtained in Ref. [27]; the curve is the fit result.

In the energy range $880\leqslant\sqrt{s}\leqslant970$ MeV (Fig. 20) the fitted curves for the second and third models exceed the experimental points on average by about 1.5σ and 1σ, respectively. The difference between models 2 and 3 is also seen in the energy regions $\sqrt{s}\leqslant720$ MeV and $\sqrt{s}\geqslant1100$ MeV (Figs. 17 and 22). The $\chi^2_{\omega\pi\pi(DM2)}$ for the third model increases by a factor of 2 in comparison with the second model. The results of the $e^+e^-\to\omega\pi^+\pi^-$ cross section fits are shown in Fig. 23. In the case when the form factors (15) are used, the theoretical curve poorly describes the experimental points at the left slope of the resonance. The CMD2 results for the $e^+e^-\to\omega\pi^+\pi^-$ reaction studies [41] are also presented in Fig. 23. These data agree better with the second model.

If the relative bias between the SND and DM2 measurements is not assumed, the $\chi^2_{3\pi(DM2)}$ value is rather large: $\chi^2_{3\pi(DM2)}/N_{fit}=(37–40)/18$. Here N_{fit} is the number of fitted experimental points (Table IV). A rather large scale factor $C=1.54$ is required to make agreement between the SND and DM2 data, and in this case $\chi^2_{3\pi(DM2)}/N_{fit}=(22–27)/18$. In order not to guess about the relative systematics between the SND and DM2 experiments, the fits described above were redone assuming $C=1$, but without taking into account the $e^+e^-\to\pi^+\pi^-\pi^0$ cross section measured in the DM2 experiments (Table V). The parameters $m_{\omega''}$, $\Gamma_{\omega''}$, and $\sigma(\omega''\to\omega\pi^+\pi^-)$ were obtained from the fitting to the cross section $e^+e^-\to\omega\pi^+\pi^-$ reported by DM2, and $m_{\omega'}$, $\Gamma_{\omega'}$, $\sigma(\omega'\to3\pi)$, and $\sigma(\omega''\to3\pi)$ were obtained by using SND data only. In this case the first model (column 1, Table V) agrees with experimental data, but agreement is significantly better if the fits are performed in the second or third models (columns 2 and 3 in Table V). The χ^2_{tot} value for the third model is slightly bigger than for the second one. In this approach the fitted curve is in conflict with the DM2 measurement of the $e^+e^-\to\pi^+\pi^-\pi^0$ cross section (Fig. 24).

VII. DISCUSSION

Comparison of the $e^+e^-\to\pi^+\pi^-\pi^0$ cross section obtained in SND experiments with other results [8,10,15–16,19] is shown in Figs. 25–28. The DM1 results [17] are in agreement with the SND measurements. The ND results [8,19] agree with the SND data in the energy region $\sqrt{s}<930$ MeV, while for $\sqrt{s}>930$ MeV the ND points lie

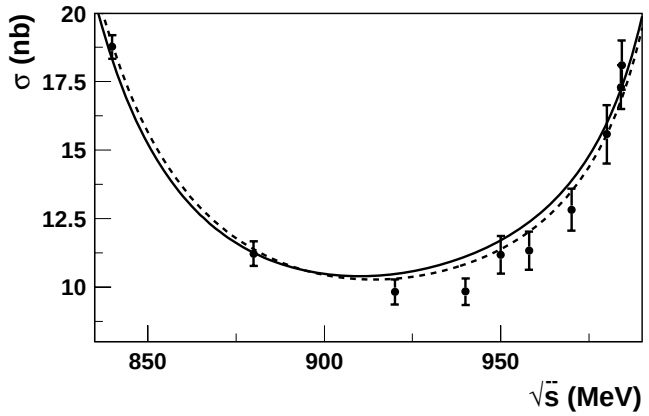

FIG. 20. The $e^+e^-\to\pi^+\pi^-\pi^0$ cross section. Dots are the SND data obtained in this work and in Refs. [2,27]. The curves are results of fitting to the data in model 2 (solid curve) and in model 3 (dashed curve).

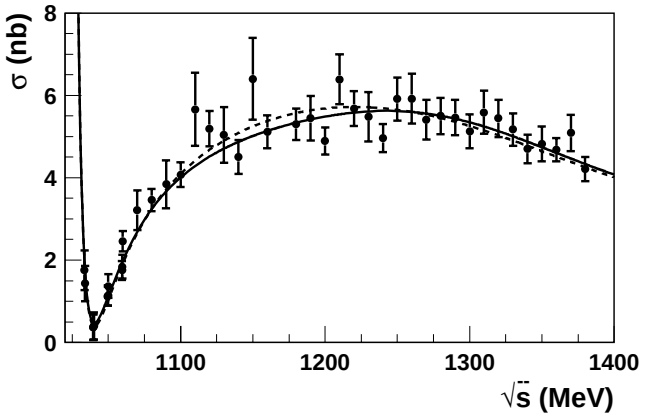

FIG. 22. The $e^+e^-\to\pi^+\pi^-\pi^0$ cross section. Dots are the experimental data obtained in Refs. [2,27]. The curves are results of fitting to the data in model 2 (solid curve) and in model 3 (dashed curve).

TABLE V. Fit results for the $e^+e^-\to\pi^+\pi^-\pi^0$, and $\omega\pi^+\pi^-$ cross sections. The DM2 data for $e^+e^-\to\pi^+\pi^-\pi^0$ were not used. The column number N corresponds to the different models for the $A_{\rho\pi}$ amplitude. N_{fit} is the number of fitted points. The first error is statistical; the second error shows the difference in the fit results due to various assumptions about the $e^+e^-\to\pi^+\pi^-\pi^0$ reaction dynamics.

	N		
	1	2	3
m_ω (MeV)	782.76 ± 0.08	782.72 ± 0.08	782.74 ± 0.08
Γ_ω (MeV)	$8.63\pm0.04\pm0.01$	$8.71\pm0.04\pm0.01$	8.65 ± 0.04
$\sigma(\omega\to3\pi)$ (nb)	$1608\pm7\pm1$	$1618\pm10\pm2$	$1612\pm7\pm2$
$\sigma(\phi\to3\pi)$ (nb)	$653\pm6\pm4$	$652\pm8\pm5$	$665\pm10\pm8$
$\phi_{\omega\phi}$ (deg)	$166\pm3\pm3$	$165\pm3\pm4$	$195\pm6\pm5$
r_0 (GeV^{-1})			$2.3^{+1.2}_{-0.8}\pm0.2$
$m_{\omega'}$ (MeV)	$1273^{+25}_{-20}\pm28$	$1386^{+70}_{-50}\pm60$	$1300\pm30\pm30$
$\Gamma_{\omega'}$ (MeV)	$405^{+60}_{-50}\pm73$	$827^{+300}_{-200}\pm186$	$595\pm50\pm50$
$\sigma(\omega'\to3\pi)$ (nb)	$6.9\pm0.4\pm0.7$	$5.0\pm1.0\pm0.5$	$5.6\pm0.3\pm0.5$
$m_{\omega''}$ (MeV)	$1819^{+90}_{-50}\pm32$	$1773^{+40}_{-30}\pm12$	$1758\pm20\pm5$
$\Gamma_{\omega''}$ (MeV)	$679^{+450}_{-200}\pm121$	$505^{+150}_{-100}\pm35$	$345\pm50\pm10$
$\sigma(\omega''\to3\pi)$ (nb)	$5.6\pm2.0\pm1.1$	$5.7\pm1.7\pm0.6$	$7.6\pm1.6\pm1.6$
$\sigma(\omega''\to\omega\pi^+\pi^-)$ (nb)	$1.2\pm0.3\pm0.2$	$1.5\pm0.2\pm0.1$	$1.7\pm0.2\pm0.1$
$\sigma(\rho\to3\pi)$ (nb)		$0.083^{+0.056}_{-0.033}\pm0.009$	
$\phi_{\omega\rho}$ (deg)		$-134^{+17}_{-13}\pm8$	
χ^2_ω/N_{fit}	(60–63)/49	(52–55)/49	(40–42)/49
$\chi^2_{(1)}/N_{fit}$	(10–16.6)/6	(11.9–13)/6	(4.6–6.3)/6
$\chi^2_{(SND)}/N_{fit}$	(69–74)/67	(51–52)/67	(52–56)/67
$\chi^2_{3\pi(DM2)}/N_{fit}$	—	—	—
$\chi^2_{\omega\pi\pi(DM2)}/N$	(11–14)/18	10/18	23/18
χ^2_{tot}/N_{fit}	(139–149)/134	(112–118)/134	(115–120)/134

about 2σ lower than the SND ones. In the vicinity of the ω resonance peak ($\sqrt{s}\simeq780$ MeV) the SND cross section exceeds the CMD2 measurements [10], while in the ϕ meson energy region the SND and CMD2 results [15,16] are in agreement.

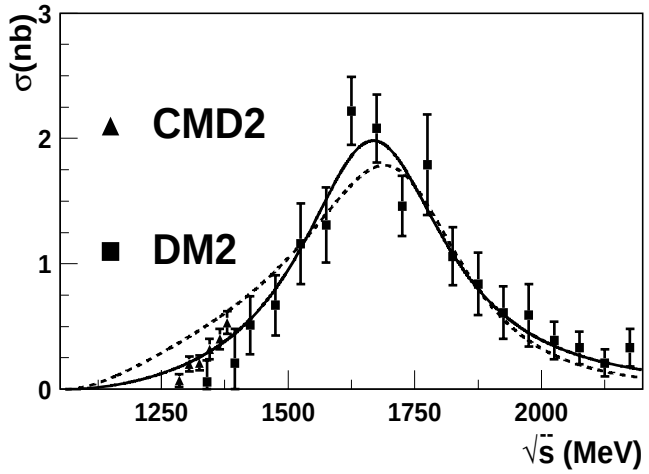

FIG. 23. The $e^+e^-\to\omega\pi^+\pi^-$ cross section. The results of the DM2 [25] and CMD2 [41] experiments are shown. The curves are results of fitting to the DM2 data in model 2 (solid curve) and in model 3 (dashed curve).

The ω meson parameters m_ω, Γ_ω, and $\sigma(\omega\to3\pi)$ were measured through study of the $e^+e^-\to\pi^+\pi^-\pi^0$ cross section. The ω meson mass was found to be

$$m_\omega=782.79\pm0.08\pm0.09\ \text{MeV}.$$

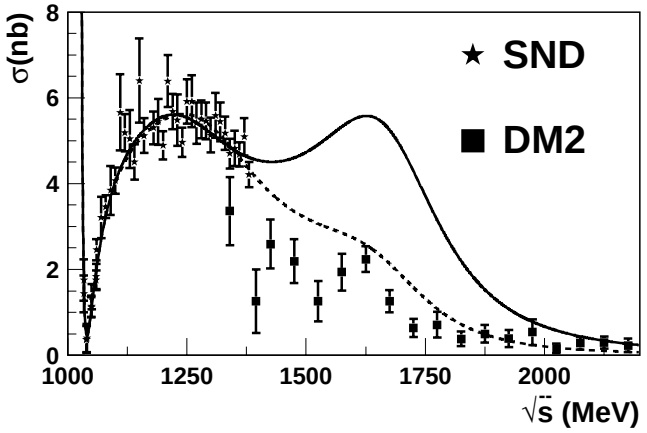

FIG. 24. The $e^+e^-\to\pi^+\pi^-\pi^0$ cross section. The results of the SND [2,27] and DM2 [25] experiments are shown. The curves are results of fitting to the data in model 2. The dashed curve corresponds to the fit under the assumption that a relative bias between the SND and DM2 data exists (DM2 data were scaled by a factor of $C=1.54$). The solid curve is the result of fitting to the SND data only.

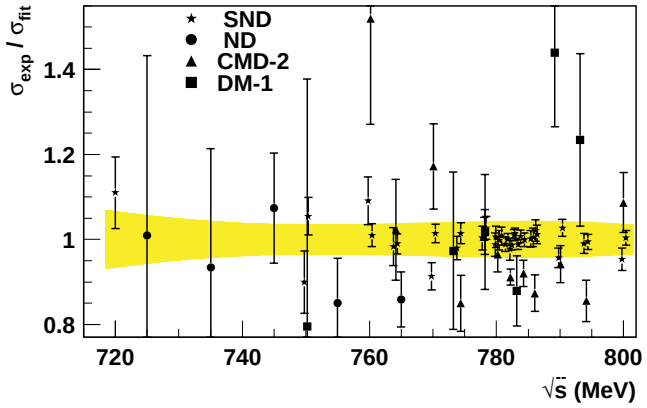

FIG. 25. The ratio of the $e^+e^-\to\pi^+\pi^-\pi^0$ cross section obtained in different experiments to the fit curve. The shaded area shows the systematic error of the SND measurements. The SND (this work), DM1 [17], ND [8,19], and CMD2 [10] results are presented.

Here the systematic error is related to the accuracy of the VEPP-2M energy scale calibration by the resonant depolarization method, 0.04 MeV, and to the model uncertainty, 0.08 MeV. The SND measurement in comparison with the results of experiments [6,10,17,42–44] and the world average value m_ω [1] is shown in Fig. 29. The SND result is in agreement with the CMD2 measurement [10], and differs from the world average by about 1.3 standard deviations. The maximum difference, about 3.4 standard deviations, is between the SND result and the Crystal Barrel measurement $m_\omega = 781.96 \pm 0.21$ [43].

The following value of the ω meson width was obtained:

$$\Gamma_\omega = 8.68 \pm 0.04 \pm 0.15 \ \text{MeV}.$$

The systematic error is related to the model dependence and to the accuracy of the energy determination. The comparison of this value with the results obtained in Refs. [5–7,9,10,17,42] and with the Particle Data Group (PDG)

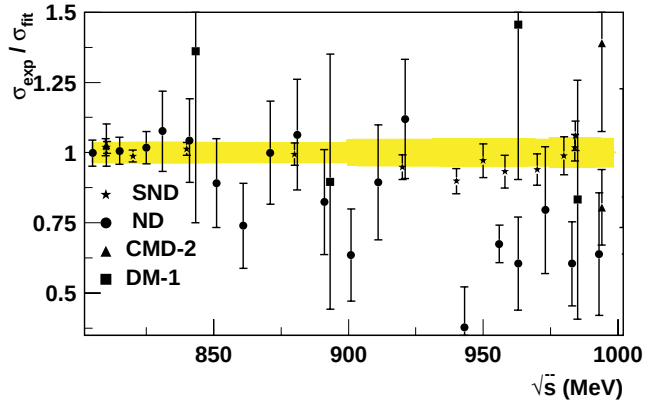

FIG. 26. The ratio of the $e^+e^-\to\pi^+\pi^-\pi^0$ cross section obtained in different experiments to the fit curve. The shaded area shows the systematic error of the SND measurements. The SND (this work and Refs. [2,27]) DM1 [17], ND [8,19], and CMD2 [15,16] results are presented.

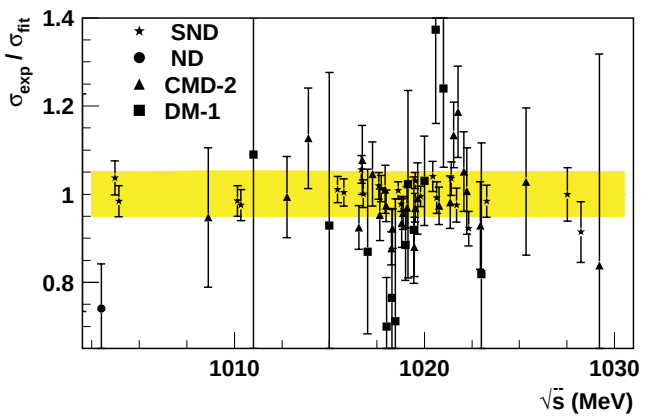

FIG. 27. The ratio of the $e^+e^-\to\pi^+\pi^-\pi^0$ cross section obtained in different experiments to the fit curve. The shaded area shows the systematic error of the SND measurements. The SND [27], DM1 [17], ND [8,19], and CMD2 [15,16] results are presented.

world average value [1] is shown in Fig. 30. The SND result agrees with other measurements.

The parameter $\sigma(\omega\to 3\pi)$ was found to be

$$\sigma(\omega\to 3\pi) = 1615 \pm 9 \pm 57 \ \text{nb}.$$

The systematic error includes the systematic uncertainties in the detection efficiency and luminosity determinations, 55 nb in total, and the model dependence, 13 nb. A comparison of the value obtained with other experimental results [5–7,9,10,17] and with the PDG world average [1] is shown in Fig. 31. The SND result exceeds the central values of the majority of the previous measurements. It differs by less than 1 standard deviation from the results in Refs. [7,9,5], by about 1.4 standard deviations from the DM1 measurement [17], and by 2 standard deviations from the OLYA result [6] and the PDG world average $\sigma(\omega\to 3\pi) = 1484 \pm 29$ nb. The difference from the most precise measurements, done by CMD2 [10] and SND, is about 2.5 standard deviations.

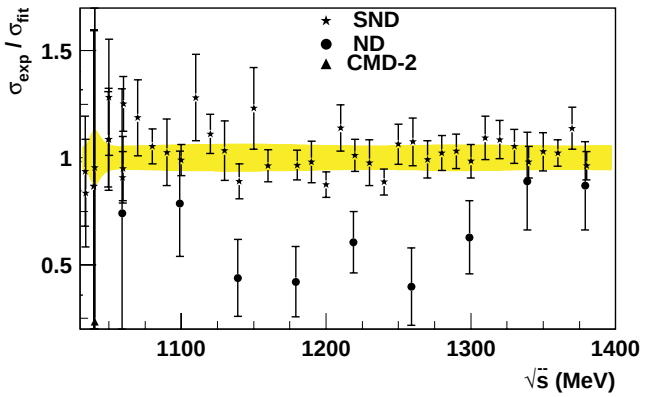

FIG. 28. The ratio of the $e^+e^-\to\pi^+\pi^-\pi^0$ cross section obtained in different experiments to the fit curve. The shaded area shows the systematic error of the SND measurements. The SND [2,27], ND [8,19], and CMD2 [16] results are presented.

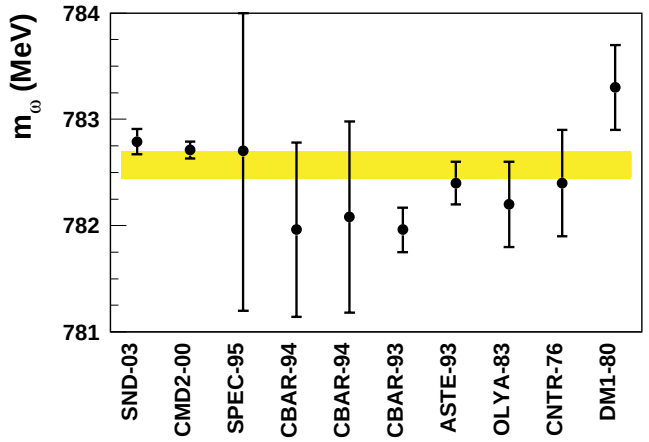

FIG. 29. The ω meson mass m_ω measured in this work (SND-03) and in Refs. [6,10,17,42–44]. The shaded area shows the world average value [1].

Using the SND result $\sigma(\omega\to\pi^0\gamma)=155.8\pm2.7\pm4.8$ nb [37], the ratio of the partial widths of the $\omega\to\pi^0\gamma$ and $\omega\to3\pi$ decays was calculated:

$$\frac{\Gamma(\omega\to\pi^0\gamma)}{\Gamma(\omega\to3\pi)}=0.097\pm0.002\pm0.005.$$

This value agrees with the PDG world average [1] and with other experimental results [5,7,44–46] (Fig. 32).

Using $\sigma(\omega\to3\pi)$, measured in this work, the SND result of the $\omega\to\pi^0\gamma$ decay study [37] and the PDG world average value $B(\omega\to\pi^+\pi^-)=0.0170\pm0.0028$ [1], the partial width of the $\omega\to e^+e^-$ decay, and the ω meson main decays branching ratios were obtained:

$$\Gamma(\omega\to e^+e^-)=0.653\pm0.003\pm0.021\ \text{keV},$$

$$B(\omega\to e^+e^-)=(7.52\pm0.04\pm0.24)\times10^{-5},$$

$$B(\omega\to3\pi)=0.8965\pm0.0016\pm0.0048,$$

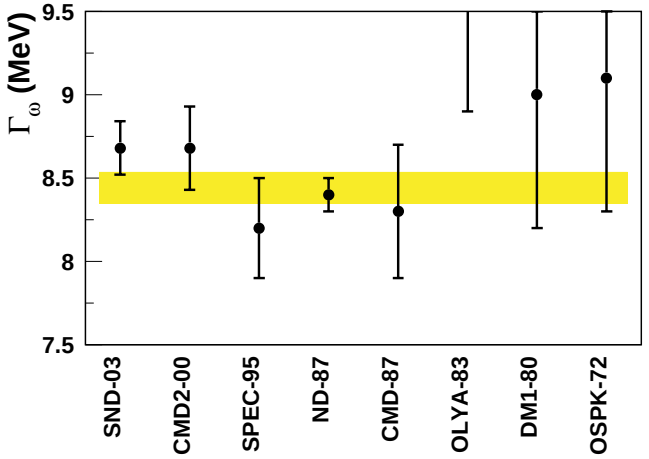

FIG. 30. The ω meson width Γ_ω measured in this work (SND-03) and in Refs. [5–7,9,10,17,42]. The shaded area shows the world average value [1].

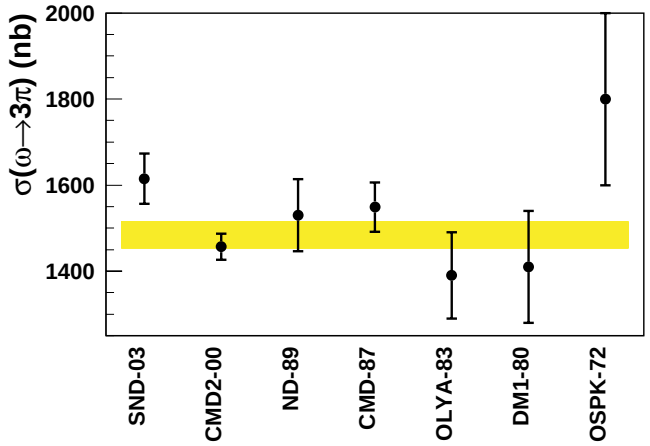

FIG. 31. The value of $\sigma(\omega\to3\pi)$ measured in this work (SND-03) and in Refs. [5–7,9,10,17]. The shaded area shows the world average value [1].

$$B(\omega\to\pi^0\gamma)=0.0865\pm0.0016\pm0.0042.$$

A comparison of these results with the PDG data [1] is presented in Table VI. The value of $B(\omega\to e^+e^-)$, calculated by using the SND data, exceeds the world average by about 2 standard deviations (by 8%).

The $e^+e^-\to\pi^+\pi^-\pi^0$ and $e^+e^-\to\omega\pi^+\pi^-$ cross section analyses show that the data cannot be described by a sum of ω,ϕ mesons and two ω',ω'' resonances (model 1). The data can be satisfactorily described with model 3, which takes into account the form factors (15), with constrained partial width growth with energy. The range parameter of this form factor was found to be

$$r_0=2.5^{+1.1}_{-0.8}\pm0.5\ \text{GeV}^{-1}.$$

This agrees with the expected vector meson effective ''radius'' 2.5–3 GeV^{-1} [47]. The second error is due to model dependence. Model 2, which takes into account the $\gamma^\star\to\rho$

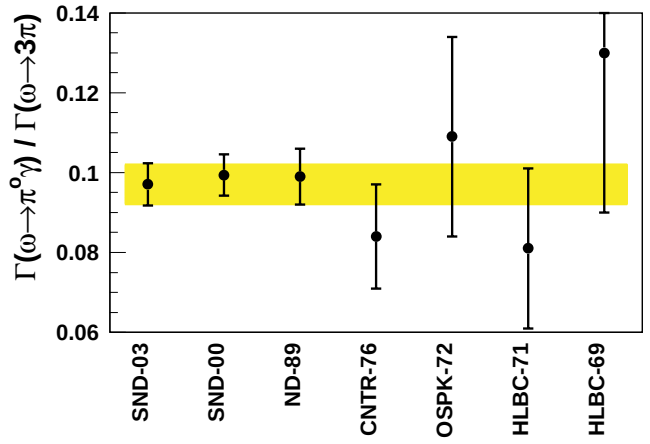

FIG. 32. The ratio of the partial widths $\omega\to\pi^0\gamma$ and $\omega\to3\pi$, obtained in this work (SND-03) and in Refs. [5,7,44–46]. The shaded area shows the world average value [1].

TABLE VI. Comparison of the $\omega\to 3\pi$, $\pi^0\gamma$, and e^+e^- decay branching ratios obtained by using the SND data with the world averages [1].

	SND	PDG 2002
$B(\omega\to e^+e^-)$	$(7.52\pm 0.24)\times 10^{-5}$	$(6.95\pm 0.15)\times 10^{-5}$
$B(\omega\to 3\pi)$	0.8965 ± 0.0051	0.8910 ± 0.007
$B(\omega\to\pi^0\gamma)$	0.0865 ± 0.0045	0.087 ± 0.004

$\to 3\pi$ transition, also satisfactorily describes the experimental data. For the parameters of this model, the following values were obtained:

$$\sigma(\rho\to 3\pi)=0.112^{+0.060}_{-0.040}\pm 0.038 \text{ nb},$$

$$\phi_{\omega\rho}=-135^{+17}_{-13}\pm 9^\circ.$$

Here the systematic error is due to model uncertainty. The $\sigma(\rho\to 3\pi)$ value given above corresponds to the branching ratio $B(\rho\to 3\pi)=(1.01^{+0.54}_{-0.36}\pm 0.34)\times 10^{-4}$. Assuming that the $\rho\to 3\pi$ transition proceeds via the ρ-ω mixing mechanism, the following values of the $\gamma^\star\to\rho\to 3\pi$ process parameters are expected: $\phi_{\omega\rho}\simeq -90^\circ$ and $\sigma(\rho\to 3\pi)=0.05$–$0.07$ nb. The $\sigma(\rho\to 3\pi)$ value obtained in the analysis agrees with the expected one, while $\phi_{\omega\rho}$ differs from the expected value by about two standard deviations. Let us note that the $\sigma(\rho\to 3\pi)$ values have to be interpreted as $\sigma(\rho\to 3\pi)=(0.112^{+0.060}_{-0.040})\times C_{scale}$ nb, where $C_{scale}=0.66$–1.34.

In general, model 2 seems to be preferable to model 3 due to the following considerations. The full data set for the $e^+e^-\to\pi^+\pi^-\pi^0$ and $\omega\pi^+\pi^-$ cross sections is in somewhat better agreement with the second model. Approximation of the $e^+e^-\to\omega\pi^+\pi^-$ cross section using the third model is poor (Fig. 23). The $\phi_{\omega\phi}$ phase value, obtained by the fit in the second model agrees with the theoretical prediction $\phi_{\omega\phi}=\Psi(m_\phi)\approx 160^\circ$ [39], while the phase $\phi_{\omega\phi}$, obtained by using the third model, exceeds the expected value (Fig. 33). But, unfortunately, the available experimental data are insufficient to draw a strict conclusion about observation of the $\rho\to 3\pi$ decay.

The parameter $\sigma(\phi\to 3\pi)$ was found to be

$$\sigma(\phi\to 3\pi)=657\pm 10\pm 37 \text{ nb}.$$

The systematic error includes the systematic uncertainties in the detection efficiency and luminosity determinations, 33 nb in total, and the model dependence, 17 nb. This value agrees with the results of our previous analysis [2,27]. The SND result also agrees with other measurements [8,11,12,14–18] and with the PDG world average [48] (Fig. 34).

The fit within the models 2 and 1 (Tables IV and V) gave the result

$$\phi_{\omega\phi}=163\pm 3\pm 6^\circ.$$

The systematic error is related to model dependence. The result obtained is in agreement with the theoretical prediction (Fig. 33) $\phi_{\omega\phi}=\Psi(s),\Psi(m_\phi)=163^\circ$, which takes into account the ϕ-ω mixing [39]. The fits with model 3 (column 3 in Tables IV and V) gave the result $\phi_{\omega\phi}=190\pm 5\pm 10^\circ$, which exceeds the theoretical prediction.

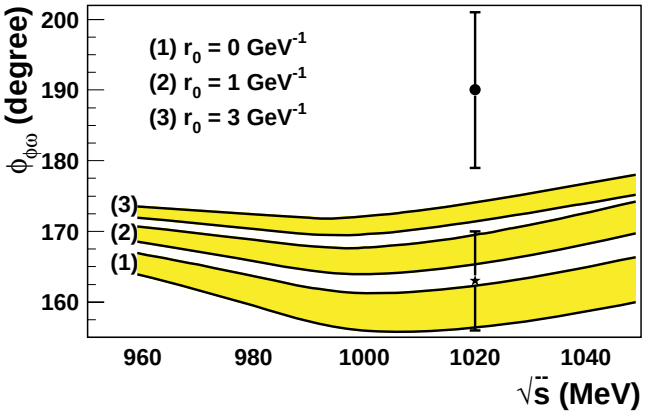

FIG. 33. The phase $\phi_{\omega\phi}$ obtained in this work. The star and the dot indicate the phase values obtained from the fit in the second and third models, respectively. The shaded areas show the expected energy behavior of the $\phi_{\omega\phi}$ phase [39] for various values of the range parameter r_0.

The conventional view on the OZI suppressed $\phi\to\pi^+\pi^-\pi^0$ decay is that it proceeds through ϕ-ω mixing, i.e., in the wave function of the ϕ meson, which is dominated by s quarks, there is an admixture of u and d quarks:

$$|\phi\rangle\approx|\phi^{(0)}\rangle+\varepsilon_{\phi\omega}|\omega^{(0)}\rangle,\quad |\phi^{(0)}\rangle=s\bar{s},$$

$$|\omega^{(0)}\rangle=(u\bar{u}+d\bar{d})/\sqrt{2}.$$

$\varepsilon_{\phi\omega}\approx 0.05$ is the ϕ-ω mixing parameter. An alternative to the ϕ-ω mixing is the direct decay. In Refs. [34,36,49–51] it was shown that there are no serious reasons to prefer the ϕ-ω mixing to the direct transition, and methods of determination of the $\phi\to\pi^+\pi^-\pi^0$ decay mechanism were suggested. In particular, it was proposed in Ref. [51] to analyze the $\Gamma(\phi\to e^+e^-)/\Gamma(\omega\to e^+e^-)$ ratio. In this work, $B(\omega$

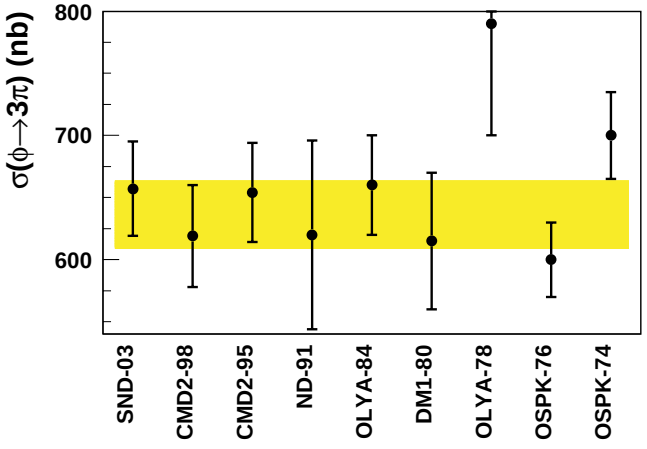

FIG. 34. The value of $\sigma(\phi\to 3\pi)$ obtained in this work (SND-03) and in Refs. [8,11,12,14–18]. The shaded area shows the world average value according to the year 2000 PDG table [48].

$\to e^+e^-$) based mainly on the SND data was obtained, and in Ref. [27] $B(\phi\to e^+e^-)$ was measured by SND. We performed the analysis of the ϕ and ω meson to lepton width ratio based on the SND data only. To improve the accuracy of the $B(\phi\to e^+e^-)$ determination, the SND results for the $\phi\to\mu^+\mu^-$ decay [52] were used. The average of these measurements $\sqrt{B(\phi\to e^+e^-)B(\phi\to\mu^+\mu^-)}=(2.93\pm0.11)\times10^{-4}$ agrees with $B(\phi\to e^+e^-)=(2.93\pm0.15)\times10^{-4}$ [27]. Assuming $B(\phi\to e^+e^-)=B(\phi\to\mu^+\mu^-)$, one gets $B(\phi\to e^+e^-)=(2.93\pm0.09)\times10^{-4}$. The ratio of the leptonic widths is equal to

$$R_{e^+e^-}=\frac{\Gamma(\phi\to e^+e^-)}{\Gamma(\omega\to e^+e^-)}=1.89\pm0.08.$$

On the other hand, this ratio can be written in the following form:

$$R_{e^+e^-}=\left(\frac{m_\omega}{m_\phi}\right)^3\left|\frac{g^{(0)}_{\gamma\phi}+\varepsilon_{\phi\omega}g^{(0)}_{\gamma\omega}}{g^{(0)}_{\gamma\omega}-\varepsilon_{\phi\omega}g^{(0)}_{\gamma\phi}}\right|^2. \tag{22}$$

Using the $R_{e^+e^-}$ value obtained, Eq. (22), and the nonrelativistic quark model prediction

$$\frac{f^{(0)}_\omega}{f^{(0)}_\phi}=-\sqrt{2}\quad\left(f_V=\frac{\sqrt{\alpha}m_V^2}{g_{\gamma V}}\right),$$

the ϕ-ω mixing parameter $\varepsilon_{\phi\omega}\approx0.06$ was obtained. On the other hand, taking into account the equation $g_{\phi\rho\pi}=g^{(0)}_{\phi\rho\pi}+\varepsilon_{\phi\omega}g^{(0)}_{\omega\rho\pi}$, and assuming $g^{(0)}_{\phi\rho\pi}=0$ and $g^{(0)}_{\omega\rho\pi}=g_{\omega\rho\pi}$, we found $\varepsilon_{\phi\omega}\approx0.06$. Here the $g_{\omega\rho\pi}$ and $g_{\phi\rho\pi}$ coupling constants were calculated by using the SND results obtained in this work and in Ref. [27], and the phase space factors $W_{\rho\pi}(m_\omega)$ and $W_{\rho\pi}(m_\phi)$ were calculated assuming $s_1=0$ and $a_{3\pi}=0$. In this case the SND data agree with the ϕ-ω mixing dominance in the $\phi\to\pi^+\pi^-\pi^0$ decay.

The ratio $f^{(0)}_\omega/f^{(0)}_\phi=-\sqrt{2}$ is valid if the $\psi(0,m_V)$ wave function of the $q\bar{q}$ bound state at the origin behaves like $|\psi(0,m_V)|^2\propto m_V^3$, that is, it corresponds to the Coulomb-like nonrelativistic potential. But experimental data on the vector meson ρ, ω, ϕ, J/ψ, and $\Upsilon(1S)$ leptonic widths support the $|\psi(0,m_V)|^2\propto m_V^2$ behavior. Indeed, according to Ref. [53],

$$\Gamma(V\to e^+e^-)=\frac{16\pi\alpha^2}{m_V^2}C_V^2|\psi(0,m_V)|^2,$$

where C_V is the mean electric charge of the valence quarks inside the vector meson V ($C_\rho^2=1/2$, $C_\omega^2=1/18$, $C_\phi^2=1/9$, $C_{J/\psi}^2=4/9$, $C_{\Upsilon(1S)}^2=1/9$). In the case of $|\psi(0,m_V)|^2\propto m_V^2$, and in the absence of mixing, the following ratios are expected:

$$\begin{aligned}&\Gamma(\rho\to e^+e^-):\Gamma(\omega\to e^+e^-):\Gamma(\phi\to e^+e^-):\Gamma\\&\quad\times(J/\psi\to e^+e^-):\Gamma(\Upsilon(1S)\to e^+e^-)\\&=C_\rho^2:C_\omega^2:C_\phi^2:C_{J/\psi}^2:C_{\Upsilon(1S)}^2\\&=4.5:0.5:1:4:1.\end{aligned}\tag{23}$$

Using the SND $\Gamma(\omega\to e^+e^-)$ and $\Gamma(\phi\to e^+e^-)$ values and the world average for $\Gamma(\rho\to e^+e^-)$, $\Gamma(J/\psi\to e^+e^-)$, and $\Gamma(\Upsilon(1S)\to e^+e^-)$ [1], we have found

$$\begin{aligned}&\Gamma(\rho\to e^+e^-):\Gamma(\omega\to e^+e^-):\Gamma(\phi\to e^+e^-):\Gamma\\&\quad\times(J/\psi\to e^+e^-):\Gamma(\Upsilon(1S)\to e^+e^-)\\&=5.2\pm0.2:0.495\pm0.025:0.93\pm0.05:3.98\pm0.032:1.\end{aligned}\tag{24}$$

These ratios agree with the expected Eq. (23). If $|\psi(0,m_V)|^2\propto m_V^2$, then $f^{(0)}_\omega/f^{(0)}_\phi=-\sqrt{2m_\omega/m_\phi}$ and by using Eq. (22) $\varepsilon_{\phi\omega}\approx0.015$ can be obtained. In this case the coupling constant of the direct $\phi\to\pi^+\pi^-\pi^0$ decay $g^{(0)}_{\phi\rho\pi}\approx0.7\cdot g_{\phi\rho\pi}$ is required to describe the experimental value for $B(\phi\to3\pi)$, indicating the direct transition as the main mechanism of the decay.

The following ω' parameters were obtained from the fits (Tables IV and V):

$$m_{\omega'}=1400\pm50\pm130\ \text{MeV},$$

$$\Gamma_{\omega'}=870^{+500}_{-300}\pm450\ \text{MeV},$$

$$\sigma(\omega'\to3\pi)=4.9\pm1.0\pm1.6\ \text{nb}.$$

The ω' decays mostly into $\pi^+\pi^-\pi^0$ and its electronic width is $\Gamma(\omega'\to e^+e^-)\sim570$ eV. The ω'' parameters were found to be

$$m_{\omega''}=1770\pm50\pm60\ \text{MeV},$$

$$\Gamma_{\omega''}=490^{+200}_{-150}\pm130\ \text{MeV},$$

$$\sigma(\omega''\to3\pi)=5.4^{+2.0}_{-0.4}\pm3.9\ \text{nb},$$

$$\sigma(\omega''\to\omega\pi^+\pi^-)=1.9\pm0.4\pm0.6\ \text{nb}.$$

The ω'' resonance decays with approximately equal probability into $\pi^+\pi^-\pi^0$ and $\omega\pi\pi$: $B(\omega''\to3\pi)\sim0.65$, $B(\omega''\to\omega\pi\pi)\sim0.35$, and it has the electronic width $\Gamma(\omega''\to e^+e^-)\sim860$ eV. The second errors shown above are due to the model uncertainty and possible bias between the SND and DM2 measurements. The ω' and ω'' parameters obtained in this work are somewhat different from those obtained in our previous analysis [2]. In particular, the ω' and ω'' full width values have decreased a little. This difference is attributed to the fact that new data for the $e^+e^-\to\pi^+\pi^-\pi^0$ cross section below 1 GeV were added in the fits. Of course, the values obtained are not precise measurements; they should be considered rather as an approximate estimation of the ω' and ω'' resonance main parameters.

In the energy region $880\leqslant\sqrt{s}\leqslant970$ MeV, the experimental points deviate from the fitting curves (Fig. 20). The difference can be attributed to inadequacy of the applied theoretical models, and uncertainty of the ω' and ω'' resonances contributions. Maybe a more accurate consideration of the vector meson mixing is required.

Using the $e^+e^-\to\pi^+\pi^-\pi^0$ cross section, obtained with the SND detector in this work and in Refs. [2,27], the contribution to the anomalous magnetic moment of the muon, due to the $\pi^+\pi^-\pi^0$ intermediate state in the vacuum polarization, was calculated via the dispersion integral:

$$a_\mu(3\pi,\sqrt{s}<1.38\ \text{GeV})=\left(\frac{\alpha m_\mu}{3\pi}\right)^2\int_{s_{min}}^{s_{max}}\frac{R(s)K(s)}{s^2}ds,$$

where $s_{max}=1.38$ GeV, $s_{min}=m_{\pi^0}+2m_\pi$, $K(s)$ is the QED kernel, and

$$R(s)=\frac{\sigma(e^+e^-\to\pi^+\pi^-\pi^0)\cdot[1-\Delta_l(s)-\Delta_h(s)]^2}{\sigma(e^+e^-\to\mu^+\mu^-)},$$

$$\sigma(e^+e^-\to\mu^+\mu^-)=\frac{4\pi\alpha}{3s}.$$

Here $\sigma(e^+e^-\to\pi^+\pi^-\pi^0)$ is the experimental cross section, and $\Delta_l(s)$ and $\Delta_h(s)$ are corrections due to the leptonic and hadronic vacuum polarizations. The $\Delta_l(s)$ was calculated according to Ref. [54] and $\Delta_h(s)$ was obtained by using the $e^+e^-\to$hadrons total cross section.

The integral was evaluated by using the trapezoidal rule. To take into account the numerical integration errors, the correction method suggested in Ref. [55] was applied. As a result, we obtained

$$a_\mu(3\pi,\sqrt{s}<1.38\ \text{GeV})=(458\pm2\pm17)\times10^{-11}.$$

At present, at BINP (Novosibirsk) a VEPP-2000 collider with energy range from 0.36 to 2 GeV and luminosity up to $10^{32}\ \text{cm}^{-2}\,\text{s}^{-1}$ (at $\sqrt{s}\sim2$ GeV) is under construction [56]. The $e^+e^-\to\pi^+\pi^-\pi^0$ process studies in the energy region $\sqrt{s}<2$ GeV will be continued in future experiments with the SND detector at this new facility.

VIII. CONCLUSION

The cross section of the process $e^+e^-\to\pi^+\pi^-\pi^0$ was measured in the SND experiment at the VEPP-2M collider in the energy region $\sqrt{s}$ below 980 MeV. The measured cross section was analyzed in the framework of the generalized vector meson dominance model together with the $e^+e^-\to\pi^+\pi^-\pi^0$ and $\omega\pi^+\pi^-$ cross sections obtained by SND and DM2 in the energy region $980<\sqrt{s}<2000$ MeV. The ω meson parameters $m_\omega=782.79\pm0.08\pm0.09$ MeV, $\Gamma_\omega=8.68\pm0.04\pm0.15$ MeV, and $\sigma(\omega\to3\pi)=1615\pm9\pm57$ nb were obtained.

It was found that the experimental data cannot be described by a sum of ω, ϕ, ω', and ω'' resonance contributions. This can be interpreted as a manifestation of $\rho\to3\pi$ decay suppressed by G parity, with relative probability $B(\rho\to3\pi)=(1.01^{+0.54}_{-0.36}\pm0.034)\times10^{-4}$. The relative interference phase between the ω and ρ mesons was found to be equal to $\phi_{\omega\rho}=-135^{+17}_{-13}\pm9°$. These parameters of the $\rho\to3\pi$ decay are in agreement with the theoretical values expected from the ρ-ω mixing.

Analysis of the $\Gamma(\phi\to e^+e^-)/\Gamma(\omega\to e^+e^-)$ ratio and $g_{\phi\rho\pi}$ and $g_{\omega\rho\pi}$ coupling constants obtained in the SND experiments indicates that the direct transition is preferable to ϕ-ω mixing as the main mechanism of $\phi\to\pi^+\pi^-\pi^0$ decay.

Using the $e^+e^-\to\pi^+\pi^-\pi^0$ cross section obtained with the SND detector, the contribution to the anomalous magnetic moment of the muon due to the $\pi^+\pi^-\pi^0$ intermediate state in the vacuum polarization, was calculated: $a_\mu(3\pi,\sqrt{s}<1.38\ \text{GeV})=(458\pm2\pm17)\times10^{-11}$.

ACKNOWLEDGMENTS

The authors are grateful to N. N. Achasov for useful discussions. The present work was supported in part by Grant No. 78 1999 of the Russian Academy of Science for young scientists and by the Russian Science Support Foundation.

[1] Particle Data Group, K. Hagiwara *et al.*, Phys. Rev. D **66**, 010001 (2002).
[2] M.N. Achasov *et al.*, Phys. Rev. D **66**, 032001 (2002).
[3] N.N. Achasov, A.A. Kozhevnikov, and G.N. Shestakov, Phys. Lett. **50B**, 448 (1974); N.N. Achasov, N.M. Budnev, A.A. Kozhevnikov, and G.N. Shestakov, Yad. Fiz. **23**, 610 (1976) [Sov. J. Nucl. Phys. **23**, 320 (1976)]; N.N. Achasov and G.N. Shestakov, Fiz. Elem. Chastits At. Yadra **9**, 48 (1978).
[4] J.E. Augustin *et al.*, Phys. Lett. **28B**, 513 (1969).
[5] D. Benaksas *et al.*, Phys. Lett. **42B**, 507 (1972).
[6] L.M. Kurdadze *et al.*, Pisma Zh. Éksp. Teor. Fiz. **36**, 221 (1982) [JETP Lett. **36**, 274 (1982)].
[7] V.M. Aulchenko *et al.*, Phys. Lett. B **186**, 432 (1987); S.I. Dolinsky *et al.*, Z. Phys. C **42**, 511 (1989).
[8] S.I. Dolinsky *et al.*, Phys. Rep. **202**, 99 (1991).
[9] L.M. Barkov *et al.*, Pisma Zh. Éksp. Teor. Fiz. **46**, 132 (1987) [JETP Lett. **46**, 164 (1987)].
[10] R.R. Akhmetshin *et al.*, Phys. Lett. B **476**, 33 (2000).
[11] G. Cosme *et al.*, Phys. Lett. **48B**, 155 (1974).
[12] G. Parrour *et al.*, Phys. Lett. **63B**, 357 (1976).
[13] G. Parrour *et al.*, Phys. Lett. **63B**, 362 (1976).
[14] A.D. Bukin *et al.*, Yad. Fiz. **27**, 976 (1978) [Sov. J. Nucl. Phys. **27**, 516 (1978)].
[15] R.R. Akhmetshin *et al.*, Phys. Lett. B **364**, 199 (1995).
[16] R.R. Akhmetshin *et al.*, Phys. Lett. B **434**, 426 (1998).
[17] A. Cordier *et al.*, Nucl. Phys. **B172**, 13 (1980).
[18] L.M. Kurdadze *et al.*, Report No. Budker INP 84-7, Novosibirsk, 1984 (in Russian).
[19] A.D. Bukin *et al.*, Yad. Fiz. **50**, 999 (1989) [Sov. J. Nucl. Phys. **50**, 621 (1989)].
[20] I.B. Vasserman *et al.*, Yad. Fiz. **48**, 753 (1988) [Sov. J. Nucl. Phys. **48**, 480 (1988)].
[21] G. Cosme *et al.*, Nucl. Phys. **B152**, 215 (1979).
[22] B. Esposito *et al.*, Lett. Nuovo Cimento Soc. Ital. Fis. **28**, 195 (1980).
[23] C. Bacci *et al.*, Nucl. Phys. **B184**, 31 (1981).
[24] B. Delcourt *et al.*, Phys. Lett. **113B**, 93 (1982).
[25] A. Antonelli *et al.*, Z. Phys. C **56**, 15 (1992).
[26] M.N. Achasov *et al.*, Phys. Lett. B **462**, 265 (1999).
[27] M.N. Achasov *et al.*, Phys. Rev. D **63**, 072002 (2001).

[28] M.N. Achasov *et al.*, Phys. Rev. D **65**, 032002 (2002).
[29] M.N. Achasov *et al.*, Nucl. Instrum. Methods Phys. Res. A **449**, 125 (2000).
[30] A.N. Skrinsky, in Proceedings of the Workshop on Physics and Detectors for DAΦNE, Frascati, Italy, 1995, p. 3.
[31] A.N. Skrinsky and Yu.M. Shatunov, Sov. Phys. Usp. **32**, 548 (1989).
[32] M.N. Achasov *et al.*, Phys. Lett. B **537**, 201 (2002).
[33] N.N. Achasov and A.A. Kozhevnikov, Phys. Rev. D **49**, 5773 (1994); Yad. Fiz. **56**, 191 (1993) [Phys. At. Nucl. **56**, 1261 (1993)]; Int. J. Mod. Phys. A **9**, 527 (1994).
[34] N.N. Achasov and A.A. Kozhevnikov, Yad. Fiz. **55**, 809 (1992) [Sov. J. Nucl. Phys. **55**, 449 (1992)]; Int. J. Mod. Phys. A **7**, 4825 (1992).
[35] N.N. Achasov and A.A. Kozhevnikov, Phys. Rev. D **57**, 4334 (1998); Yad. Fiz. **60**, 2212 (1997) [Phys. At. Nucl. **60**, 2029 (1997)].
[36] N.N. Achasov *et al.*, Yad. Fiz. **54**, 1097 (1991) [Sov. J. Nucl. Phys. **54**, 664 (1991)]; Int. J. Mod. Phys. A **7**, 3187 (1992).
[37] M.N. Achasov *et al.*, Phys. Lett. B **559**, 171 (2003).
[38] M.N. Achasov *et al.*, Zh. Éksp. Teor. Fiz. **117**, 22 (2000) [JETP **90**, 17 (2000)].
[39] N.N. Achasov and A.A. Kozhevnikov, Phys. Rev. D **61**, 054005 (2000); Yad. Fiz. **63**, 2029 (2000) [Phys. At. Nucl. **63**, 1936 (2000)].
[40] E.A. Kuraev and V.S. Fadin, Yad. Fiz. **41**, 733 (1985) [Sov. J. Nucl. Phys. **41**, 466 (1985)].
[41] R.R. Akhmetshin *et al.*, Phys. Lett. B **489**, 125 (2000).
[42] R. Wurzinger *et al.*, Phys. Rev. C **51**, 443 (1995).
[43] C. Amsler *et al.*, Phys. Lett. B **327**, 425 (1994); **311**, 362 (1993); P. Weidenauer *et al.*, Z. Phys. C **59**, 387 (1993).
[44] J. Keyne *et al.*, Phys. Rev. D **14**, 28 (1976).
[45] V.M. Aulchenko *et al.*, Zh. Éksp. Teor. Fiz. **117**, 1067 (2000) [JETP **90**, 927 (2000)].
[46] A.B. Baldin *et al.*, Yad. Fiz. **13**, 1318 (1971) [Sov. J. Nucl. Phys. **13**, 758 (1971)]; F. Jacquet *et al.*, Nuovo Cimento A **63**, 743 (1969).
[47] T. Ericson and W. Wise, *Pions and Nuclei* (Clarendon Press, Oxford, 1988).
[48] Particle Data Group, D.E. Groom *et al.*, Eur. Phys. J. C **15**, 1 (2000).
[49] N.N. Achasov and A.A. Kozhevnikov, Phys. Lett. B **233**, 474 (1989).
[50] N.N. Achasov and A.A. Kozhevnikov, Yad. Fiz. **55**, 3086 (1992) [Sov. J. Nucl. Phys. **55**, 1726 (1992)]; Part. World **3**, 125 (1993).
[51] N.N. Achasov and A.A. Kozhevnikov, Phys. Rev. D **52**, 3119 (1995); Yad. Fiz. **59**, 153 (1996) [Phys. At. Nucl. **59**, 144 (1996)].
[52] M.N. Achasov *et al.*, Phys. Lett. B **456**, 304 (1999); Phys. Rev. Lett. **86**, 1698 (2001).
[53] Van Royan and V.F. Weisskopf, Nuovo Cimento A **50**, 617 (1967).
[54] A.B. Arbuzov *et al.*, J. High Energy Phys. **10**, 001 (1997).
[55] N.N. Achasov and A.V. Kiselev, Pisma Zh. Éksp. Teor. Fiz. **75**, 643 (2002) [JETP Lett. **75**, 527 (2002)].
[56] Yu.M. Shatunov *et al.*, in Proceedings of the 2000 European Particle Acceleration Conference, Vienna, 2000, p. 439.